Multiple Nitrate Source Contributions to Primary Production Inferred from Carbon and Nitrogen Isoscapes in the Southern Sea of Japan

T. Kodama[1,*], A. Nishimoto[2], K.-i. Nakamura[3,†], M. Nakae[3], N. Iguchi[3], Y. Igeta[3], and Y. Kogure[3]

[1]Fisheries Resources Institute, Japan Fisheries Research and Education Agency, Yokohama

[2]Fisheries Technology Institute, Japan Fisheries Research and Education Agency, Yokohama

[3]Fisheries Resources Institute, Japan Fisheries Research and Education Agency, Niigata

Corresponding author: Taketoshi Kodama (takekodama@g.ecc.u-tokyo.ac.jp)

[*]Present address: Graduate School of Agriculture and Life Sciences, The University of Tokyo

[†]Present address: Kokusai Kogyo Co. Ltd., Tokyo, 102-0085, Japan

Key Points:

- Intensive observations of C and N isotope ratios in the Sea of Japan demonstrate their seasonality and vertical variations.
- Variations in $\delta^{13}C$ in particulate organic matter are linked to active photosynthesis and phytoplankton growth.
- The $\delta^{15}N$ variation in particulate organic matter indicated that multiple-origin nitrate supports primary production.

Abstract

Carbon and nitrogen dynamics in the Sea of Japan (SOJ) are rapidly changing. In this study, we investigated the carbon and nitrogen isotope ratios of particulate organic matter ($\delta^{13}C_{POM}$ and $\delta^{15}N_{POM}$, respectively) at depths of ≤ 100 m in the southern part of the SOJ from 2016 to 2021. $\delta^{13}C_{POM}$ and $\delta^{15}N_{POM}$ exhibited multimodal distributions and were classified into four classes (I–IV) according to the Gaussian mixed model. A majority of the samples were classified as class II (n = 441), with mean ± standard deviation of $\delta^{13}C_{POM}$ and $\delta^{15}N_{POM}$ of –23.7 ± 1.2‰ and 3.1 ± 1.2‰, respectively. Compared to class II, class I had significant low $\delta^{15}N_{POM}$ (-2.1 ± 0.8‰, n = 11), class III had low $\delta^{13}C_{POM}$ (-27.1 ± 1.0‰, n = 21), and class IV had high $\delta^{13}C_{POM}$ (-20.7 ± 0.8‰, n = 34). A majority of the class I samples were collected in winter and had comparable temperature and salinity, indicating that Japanese local rivers contributed to class I formation. The generalized linear model demonstrated that the temperature and chlorophyll-*a* concentration all had a positive effect on $\delta^{13}C_{POM}$, supporting the hypothesis that active photosynthesis and phytoplankton growth increased $\delta^{13}C_{POM}$. However, the fluctuation in $\delta^{15}N_{POM}$ was attributed to the temperature and salinity rather than nitrate concentration. These findings suggest that multiple nitrate sources, including the East China Sea, Kuroshio, and Japanese local rivers, contribute to the primary production in the SOJ.

Plain Language Summary

Carbon and nitrogen are vital components for organisms, and their stable isotope ratios (^{13}C:^{12}C, ^{15}N:^{14}N) are useful tools for understanding their flow in the ocean. The Sea of Japan, surrounded by Japan, Korea, and Russia, is a microcosm of the ocean, where the environment is being rapidly altered by anthropogenic activities. We measured the carbon and nitrogen stable isotope ratios of small organic particles dispersed in the seawater, which are mostly phytoplankton. Carbon isotope ratios increased due to active carbon fixing and phytoplankton growth. The nitrogen isotope ratios can be classified into two clusters. The low nitrogen isotope ratio clusters were mostly found in less saline surface water in winter, indicating that they were influenced by local rivers. In the high nitrogen isotope ratio cluster, nitrogen isotope ratio was not attributed to nitrate concentration, which is a conventional key to the nitrogen isotope ratio estimation. This indicates that nitrates from other sources, in addition to deep-sea nitrate, may contribute to organic production in this sea.

1 Introduction

Carbon and nitrogen dynamics in the oceans are globally changing as a result of anthropogenic activities [*Gruber and Galloway*, 2008]. Carbon and nitrogen isotope values are particularly effective measurements for detecting changes in marine environments [*Gruber et al.*, 1999; *Ren et al.*, 2017] and ecosystems [*Lorrain et al.*, 2020]. Earth system model-based techniques have been developed at a global scale in order to comprehend the spatiotemporal variability of carbon and nitrogen isotope values [*Buchanan et al.*, 2019]. Seas that connect land and ocean are strongly affected by anthropogenic activities [*Omstedt*, 2021]. However, because current Earth system models do not focus on marginal seas, relevant information is extremely limited.

The Sea of Japan (SOJ) is a western North Pacific semi-closed marginal sea surrounded by the Korean Peninsula, the Japanese Archipelago, and the Russian coast. In the southern part of the SOJ, the Tsushima Warm Current (TWC) flows at the surface (< 200 m depth) from the

west (East China Sea) to the east (western North Pacific or the Sea of Okhotsk) throughout the year; however, this current is weak in the winter and strong in the summer, and its path exhibits complex variations [*Yabe et al.*, 2021]. The TWC governs the elemental cycles and ecosystem in the southern part of the SOJ [*Kodama*, 2020], and its water is a mixture of the Kuroshio Current, the Taiwan Warm Current, and Changjiang discharged waters [*Guo et al.*, 2006; *Isobe*, 1999]. The elemental cycles in the surface layer of the SOJ are rapidly changing, and the pH, phosphate, and oxygen concentrations have been decreasing over the past five decades [*Ishizu et al.*, 2019; *Kodama et al.*, 2016; *Ono*, 2021].

Studies in the SOJ have been undertaken using a stable isotope ratio of zooplankton and small pelagic fish tissues to determine changes in carbon and nitrogen dynamics [*Nakamura et al.*, 2022; *Ohshimo et al.*, 2021]. These studies found that the ^{13}C:^{12}C ratio in animal tissues declined at the same rate as the Suess effect, but there was no significant linear trend in the ^{15}N:^{14}N ratio [*Nakamura et al.*, 2022; *Ohshimo et al.*, 2021]. The ^{15}N:^{14}N ratio in animal tissues varies with trophic position. In the SOJ, the zooplankton biomass has been found to be negatively coupled with small pelagic fish biomass over the last half-century, and hence, food-web structure may periodically change [*Kodama et al.*, 2022a]. Thus, the baseline ^{15}N:^{14}N ratio in marine ecosystems is vital for identifying changes in nitrogen dynamics in the SOJ. However, reports on the variation in stable isotope ratios of particulate organic matter (POM) in the surface layer, which are the baseline values of marine ecosystems, are confined to the Japanese coastal areas [*Antonio et al.*, 2012; *Nakamura et al.*, 2022]. As a result, the variabilities in POM stable isotope ratios with regard to environmental parameters are not clearly understood.

Two recent studies have indicated that the carbon and nitrogen stable isotope ratio of POM varies in the western North Pacific marginal seas [*Ho et al.*, 2021; *Kodama et al.*, 2021]. The ^{13}C: ^{12}C ratio of POM increased as the phytoplankton abundance increased in the southwestern East China Sea, which is consistent with isotope fractionation that occurs during photosynthesis [*Ho et al.*, 2021]. The ^{15}N:^{14}N ratio of this area decreased with freshwater intake and coastal upwelling in the summer, and was negatively correlated with nitrate concentration [*Ho et al.*, 2021]. *Gao et al.* [2014] reported the horizontal distribution of ratios of ^{13}C:^{12}C and ^{15}N:^{14}N, and that ^{13}C:^{12}C ratio largely varies in this sea. Active nitrogen fixation decreases the ^{15}N:^{14}N ratio of POM in offshore waters in the Kuroshio area during the summer, whereas the ^{15}N:^{14}N ratio of POM remains high in the coastal waters [*Kodama et al.*, 2021].

The carbon and nitrogen isotope ratios of POM are thought to be more changeable in the SOJ than in the other western North Pacific marginal seas. In the case of carbon, *Kosugi et al.* [2016] reported that the partial pressure of CO_2 (pCO_2) on the surface of the central and eastern parts of the SOJ (312–329 μatm) differs from that in the northwestern region (360–380 μatm). Furthermore, the carbon:nitrogen ratio (C:N ratio) of POM in the surface water of the northern East China Sea is extremely high (>40:1) near Japan [*Gao et al.*, 2014], and this organic carbon-rich water may influence the carbon dynamics of the SOJ. In the case of nitrogen, primary production in the northeastern East China Sea is supported by a variety of nitrogen sources, such as atmospheric deposition, Changjiang River discharge, and Kuroshio waters with varying ^{15}N:^{14}N ratios [*Umezawa et al.*, 2021; *Umezawa et al.*, 2014]. As the decrease in phosphate concentration in the SOJ is mainly observed with an increase in the nitrogen supply in the East China Sea [*Kim et al.*, 2013; *Kodama et al.*, 2016], advection of nitrate and POM produced in the northeastern East China Sea is likely to influence the ^{15}N:^{14}N ratios in the SOJ. Previous nutrient dynamics studies have revealed that the supplied nitrate in the surface productive layer in the

SOJ originates from the Kuroshio, regeneration at the bottom of the East China Sea, the Changjiang diluted waters, and the atmosphere in the summer [*Kim et al.*, 2011; *Kodama et al.*, 2017; *Kodama et al.*, 2015]. In addition, deep mixing occurs in the SOJ in winter [*Ohishi et al.*, 2019]; thus, deep-seawater-originated nitrate contributes to the primary production as well. Although their contributions to the plankton community are limited, diazotrophs are present during the summer [*Hashimoto et al.*, 2012; *Sato et al.*, 2021]. Thus, the ^{15}N:^{14}N ratio of POM helps in identifying which nitrogen source mainly supports primary production in this sea. Therefore, in this study, we investigated the carbon and nitrogen stable isotope ratios in the southern SOJ (approximately ≤ 40°N). The main objectives were to: 1) demonstrate the spatial distribution of carbon and nitrogen stable isotope ratios, 2) understand the effects of horizontal advection of particulate organic carbon from the East China Sea, and 3) identify which nitrogen source mainly supports the primary production.

2 Materials and Methods

2.1 Sampling

POM samples with environmental data were collected from 2016 to 2021 in the southern part of the SOJ between 35°N and 41°N and between 131°15'E and 139°50'E [Figure 1] during 28 cruises using R/V *Hokko-maru*, *Shunyo-Maru*, *Yoko-Maru*, T/V *Tenyo-Maru* (Japan Fisheries Research and Education Agency), and R/V *Dai-Go Kaiyo-Maru* (Kaiyo Engineering Co., Ltd.). The cruises were held yearly from February to September, except for March [Figure 1]. The observations were repeated 14 times after 2018 along the monitoring line established off the Sado Island (SI-line) [Figure 1] (in September 2016, July 2018, August 2018, September 2018, February 2019, April 2019, June 2019, September 2019, February 2020, April 2020, June 2020, September 2020, February 2021, April 2021, and June 2021).

POM samples were generally obtained at the depths of 10 m and 30 m, or at the subsurface chlorophyll-*a* maximum (SCM). The vertical profiles of temperature, salinity, and chlorophyll-*a* fluorescence were monitored in real-time using a conductivity-temperature-depth (CTD) sensor (SBE9plus, Seabird Electronics). Real-time observations were not performed in some specific cases; here, the record-type CTD (SBE19, Seabird Electronics) without a fluorometer was used instead of the SBE9plus. On this basis, we set 30 m as the representative subsurface layer for the spring (March–June) and summer (July–September) seasons as it is below the surface mixed layer in SOJ. During the cruise in September 2020, the POM samples were collected at six depths (0, 10, 30, 50, and 100 m, and SCM) to determine the variations between the sampling layers. In the July and August cruises, photosynthetically active radiation (PAR) was occasionally accessible using a PAR sensor (Seabird Electronics) attached to the CTD. In the summer of SOJ, the mean (± SD) euphotic zone depth—where PAR is 1% of the surface—was 50 (± 14) m (n = 207), and the PAR at a depth of 30 m was 6.8 ± 4.3% of the surface. In May and August 2020, we collected samples at depths of 75 m (n = 3) and 100 m (n = 1), respectively. In spring and summer, considering the mixed layer and the euphotic zone depth, the layers at 0–10 m, 20–65 m, and 75–100 m depths were defined as the surface, subsurface, and deep layers, respectively, to detect the influence of the vertical difference of unevaluated characteristics such as light and phytoplankton community. In winter, all the samples were considered as surface layer samples because the difference in potential density between 10 and 30 m depths was <0.125 at every station, suggesting that they were within the mixed layer.

Temperature, salinity, nutrients (nitrate, nitrite, silicate, and phosphate), and chlorophyll-*a* concentrations were collected and utilized as environmental parameters at the same depth as the POM samples. Water samples were obtained using Niskin bottles mounted on a rosette or a bucket to measure nutrient, chlorophyll-*a*, and POM concentrations. The nutrient and chlorophyll-*a* concentrations were analyzed following *Kodama et al.* [2015]. The detection limits of the nutrient concentrations were 0.01–<0.05 μM for nitrite and phosphate, 0.01–<0.1 μM for nitrate, and 0.05–<0.3 μM for silicate, estimated using the standard deviations of blank values. The temperature and salinity at the 0-m depth were defined as the values observed by the CTD sensors at 1-m depth because salinity at the 0 m depth sometimes exhibited "unreliable" values. To treat the common-logarithm transformed values, the nutrient concentrations of < 0.01 μM (below the detection limit) were set as 0.01 μM.

2.2 Isotope analyses

To measure the mass and the carbon and nitrogen stable isotope ratios of the POM, 0.9–11.5 L of seawater was filtered using a pre-combusted (450°C, 6 h) glass fiber filter (pore size: 0.7 μm, GF/F, Whatman). The filtration was stopped in 2 h after sampling, and > 5 L seawater was filtered in 2 h for most of the samples. After the shipboard filtration, the samples were frozen (< –20°C). Onshore laboratory analyses were performed using methods from *Kodama et al.* [2021], whose preservation differed from that of *Lorrain et al.* [2003], while the other protocols remained the same. The carbon and nitrogen isotope ratios and their masses were determined using the same sample. The samples were exposed to HCl fumes for > 2 h to remove carbonate salt, dried in an oven (60°C) overnight and stored in a desiccator until isotope ratio measurements. After another round of oven-drying, the entire glass filter was wrapped in a tin cup. Subsequently, the carbon and nitrogen isotope ratios were measured using an Isoprime 100 isotope ratio mass spectrometer (Elementar, Langenselbold, Germany). In 2016, the colored surfaces of the glass filters were scraped off, and the carbon and nitrogen isotope ratios were measured. The absolute amounts of carbon and nitrogen in these scraped samples were different from those in the whole samples. The stable isotope ratios of carbon and nitrogen were calibrated using curves obtained from L-alanine (Shoko Science) during the measurements. The isotope compositions of carbon and nitrogen of POM sample ($\delta^{13}C_{POM}$ and $\delta^{15}N_{POM}$, respectively) were expressed using Eq. (1):

$$\delta^{13}C_{POM} \text{ or } \delta^{15}N_{POM} = (R_{sample} / R_{reference} - 1.0) \times 1000, \quad (1)$$

where R_{sample}, and $R_{reference}$ are the heavy (^{13}C and ^{15}N) to light (^{12}C and ^{14}N) isotope ratios of the POM sample and reference, respectively. The reference materials were atmospheric N_2 for nitrogen and Vienna Pee Dee Belemnite for carbon. Given the quality of the L-alanine, and $\delta^{13}C$ and $\delta^{15}N$ were rounded off to one decimal place, the precision of the analyses was within 0.2‰.

The C:N ratio of POM occasionally exhibited outliers, due to which, the mean and standard deviations (SD) of the C:N ratio were calculated and the samples whose C:N ratio differed by > 3 × SD from the mean value were eliminated. After elimination, we re-calculated the mean and SD of the C:N ratio, and the samples whose C:N ratio differed by > 3 × recalculated SD from the recalculated mean value were eliminated. Then, the samples lacking environmental data were removed. As a result, six samples were removed, and 507 samples were used in this study. Among these samples, 101 samples were obtained along the SI-line.

2.3 Statistical analyses

All statistical analyses were conducted using R [*R Core Team*, 2023]. Accompanied by the analysis of variance (ANOVA), a pairwise test with the *Tukey–Kramer* adjacent was applied to the least-squared mean (lsmean) values. The "ggeffect" package [*Lüdecke*, 2018] was used to calculate the lsmean values and SEs. The "car" package [*Fox and Weisberg*, 2018] of ANOVA was used to conduct type II ANOVA for unbalanced data comparison. Neither $\delta^{13}C_{POM}$ nor $\delta^{15}N_{POM}$ exhibited a normal distribution according to the *Kolmogorov–Smirnov* test ($p < 0.001$); both showed multimodal distributions. Therefore, we applied a two-dimensional Gaussian mixed model (GMM) to classify $\delta^{13}C_{POM}$ and $\delta^{15}N_{POM}$ using the "mclust" package [*Scrucca et al.*, 2016]. The samples were not divided based on the sampling depth and seasons. The number of classes was determined using the Bayesian information criterion (BIC).

Generalized linear models (GLMs) were applied to assess the variables that predicted the relationships between the environmental parameters and $\delta^{13}C_{POM}$ and $\delta^{15}N_{POM}$ as in *Kodama et al.* [2021]. We assumed that the error distributions of $\delta^{13}C_{POM}$ and $\delta 15N_{POM}$ were normally distributed with a linear link function in the GLMs. The full GLM models are as follows:

$$\delta X_{POM} \sim \mathrm{glm}[f(\mathrm{class}) + f(\mathrm{layer}) + f(\mathrm{season}) + \mathrm{Lon} + \mathrm{Lat} + \mathrm{C/N} + \mathrm{T} + \mathrm{S} + \mathrm{Chl} + \mathrm{Nit}] \quad (2)$$

where δX_{POM}, Lon, Lat, C/N, T, S, Chl, and Nit denote $\delta^{13}C_{POM}$ or $\delta^{15}N_{POM}$, longitude, latitude, C:N ratio, temperature, salinity, chlorophyll-*a* concentration, and nitrate concentration, respectively. The chlorophyll-*a* and nitrate concentrations were transformed into logarithmic values. The arguments of the *f* functions are categorical variables that are used to simulate non-linear relationships. The numbers of classes were defined by GMM and BIC, while those of layer and season were three each (surface, subsurface, and 100-m depth in layer and winter [January–February], spring [March–June], and summer [July–September] in season). The explanatory variables used in the full GLMs were chosen based on the retraction of multicollinearity. We also used GLM approaches that included a quadratic expression in the model, as *Nakamura et al.* [2022] did, as well as a generalized additive model approach, as *Kodama et al.* [2021] did. However, as the deviance explained values of the models did not improve, we opted for the simple GLM approach.

The explanatory variables and final GLM descriptions were selected using the corrected Akaike information criterion (AIC), which may be used to assess the likelihood of the model. The lsmean values and SEs based on the AIC-selected GLMs were used to visualize the influence of the explanatory variables on the $\delta^{13}C_{POM}$ or $\delta^{15}N_{POM}$. ANOVA was used to test the effects of the lsmean values of the categorical variables (the class, season, and depth when they remained).

Of note, we did not include the interaction terms in the GLMs. For instance, longitude–latitude interactions can reflect the 2-D variations. Moreover, the temperature–salinity (T–S) diagram is the most fundamental method for obtaining the characteristics of water masses. Therefore, although the interactions must be considered, the interaction terms of temperature and salinity could not be used instead of the T–S diagram in the GLMs. Instead of interaction terms, the classes based on the GMM were plotted on the T–S and nitrate-density (σ_t) (N-σ_t) diagrams to elucidate the effect of non-linear interactions on $\delta^{13}C_{POM}$ or $\delta^{15}N_{POM}$.

3 Results

3.1 Spatial distribution of $\delta^{13}C_{POM}$ and $\delta^{15}N_{POM}$

The $\delta^{13}C_{POM}$ and $\delta^{15}N_{POM}$ varied from –29.3 to –17.7‰ and –3.2 to 6.7‰, respectively. In September 2020, the vertical profiles (0, 10, 30, 50, and 100 m depths and SCM) of $\delta^{13}C_{POM}$ and $\delta^{15}N_{POM}$ were collected at nine stations. SCM was observed at depths of 34–56 m. The differences in the $\delta^{13}C_{POM}$, $\delta^{15}N_{POM}$, and C:N ratios were significant among the layers according to ANOVA ($p < 0.001$). The $\delta^{13}C_{POM}$ was the lowest at a depth of 50 m or SCM (mean ± SD: -25.7 ± 0.36‰ and –25.4 ± 0.45‰, respectively) [Figure 2a]. The $\delta^{13}C_{POM}$ decreased with depth of up to 50 m (or SCM layer) and slightly increased at the 100-m depth (–24.2 ± 1.26‰). The $\delta^{15}N_{POM}$ was the lowest at 10-m depth (1.5 ± 0.64‰), increased with depth, and the highest value was identified at the 100-m depth (5.0 ± 0.60‰) [Figure 2b]. The mean C:N ratio was estimated to 5.4–6.3 mol mol^{-1} except the 100-m depth with 4.2 ± 0.69 mol mol^{-1} [Figure 2c]. When the subsamples at the nine stations were regrouped into the surface (0 and 10 m depths) and subsurface (30 and 50 m and SCM) groups, the differences in both $\delta^{13}C_{POM}$ and $\delta^{15}N_{POM}$ were significant between the surface and subsurface (*t*-test, $p \leq 0.018$). Therefore, $\delta^{13}C_{POM}$ and $\delta^{15}N_{POM}$ were different between the surface and subsurface, particularly during summer.

The horizontal variations in $\delta^{13}C_{POM}$ are shown by the 1° × 1° grid median values [Figure 3a–e]. During winter, the median (± interquartile range, IQR) of the $\delta^{13}C_{POM}$ was –25.0 ± 2.34‰, and low $\delta^{13}C_{POM}$ was observed in the offshore waters (median ± IQR: –25.6 ± 3.20‰). During spring, low $\delta^{13}C_{POM}$ was identified offshore, and the surface $\delta^{13}C_{POM}$ (–24.6 ± 1.55‰) was lower than that of the subsurface (–23.7 ± 1.68‰, *Wilcoxon* test, W = 271, $p = 0.021$). During summer, the surface $\delta^{13}C_{POM}$ (–22.9 ± 1.07‰) was significantly higher than that of the subsurface (–24.4 ± 1.86‰, *Wilcoxon* test, W = 36002, $p < 0.001$). The $\delta^{13}C_{POM}$ in the subsurface during the summer was higher in the western than in the eastern part, while those of the surface were higher in the eastern than in the western part.

The horizontal variations in $\delta^{15}N_{POM}$ are shown in the same manner as $\delta^{13}C_{POM}$ [Figure 3f–i]. Evidently, in winter, lower values (~ –2.0‰) were observed in the coastal area. $\delta^{15}N_{POM}$ was higher in spring than in winter (3.12 ± 2.02‰ and 3.12 ± 2.02‰ in the surface and subsurface, respectively). Moreover, during spring, the $\delta^{15}N_{POM}$ value in the offshore area was lower than that of the coastal area. In summer, the surface $\delta^{15}N_{POM}$ (2.76 ± 1.68‰) was significantly lower than that of the subsurface (3.14 ± 1.39‰, *Wilcoxon* test, W = 19187, $p = 0.02874$). Furthermore, lower $\delta^{15}N_{POM}$ values were identified in the offshore water, and high $\delta^{15}N_{POM}$ values were observed in the coastal area of the northern part.

3.2 Temporal variations of $\delta^{13}C_{POM}$ and $\delta^{15}N_{POM}$ along the SI-line

The monthly variations in $\delta^{13}C_{POM}$ and $\delta^{15}N_{POM}$ were evaluated using the samples collected along the SI-line [Figure 4a–d]. When the interannual variations were ignored, $\delta^{13}C_{POM}$ was the lowest in April (lsmean ± SE: –26.1 ± 0.62‰) and highest in September (–22.4 ± 0.32‰) [Figure 4a]; no significant difference was observed during February, April, and June (Pairwise test with *Tukey–Kramer* adjacent, $p > 0.05$). The $\delta^{15}N_{POM}$ in the surface layer was the lowest in February (–0.5 ± 0.40‰) and highest in June (2.7 ± 0.52‰), while a significant difference was not observed among June, July, and September [Figure 4b]. In the subsurface layer, the monthly variation of $\delta^{13}C_{POM}$ was not significant (ANOVA, $p = 0.09$) [Figure 4c], and

that of $\delta^{15}N_{POM}$ was significant ($p = 0.026$) but was not significant as per the pairwise test with *Tukey–Kramer* adjacent ($p > 0.05$) [Figure 4d].

The surface $\delta^{13}C_{POM}$ and $\delta^{15}N_{POM}$ from July–September exhibited significant interannual variation (ANOVA, $p < 0.05$). The significant difference in interannual lsmean $\delta^{13}C_{POM}$ (pairwise test with *Tukey–Kramer* adjacent, $p = 0.036$) was observed between 2019 (highest: –21.9 ± 0.35‰) and 2018 (lowest: –23.5 ± 0.35‰). The interannual lsmean $\delta^{15}N_{POM}$ was the lowest in 2019 (1.5 ± 0.31‰), and significantly different (pairwise test with *Tukey–Kramer* adjacent, $p = 0.016$) from that in 2018 (3.0 ± 0.36‰). In the other combinations, there was no significant difference in the pairwise test. The temperature, salinity, and chlorophyll-*a* concentration in the surface during summer did not vary significantly (ANOVA, $p > 0.1$).

3.4 Classifications of $\delta^{13}C_{POM}$ and $\delta^{15}N_{POM}$

Furthermore, $\delta^{13}C_{POM}$ and $\delta^{15}N_{POM}$ were divided into four classes (I–IV) according to the two-dimensional GMM [Figure 5]. The mean ± SDs of $\delta^{13}C_{POM}$ and $\delta^{15}N_{POM}$ were –24.6 ± 1.2‰ and –2.1 ± 0.8‰ in class I ($n = 11$), –23.7 ± 1.2‰ and 3.1 ± 1.2‰ in class II ($n = 441$), –27.1 ± 1.0‰ and 2.0 ± 1.3‰ in class III ($n = 21$), and –20.7 ± 0.8‰ and 1.7 ± 1.0‰ in class IV ($n = 34$), respectively [Figure 5b–c]. The $\delta^{13}C_{POM}$ values were significantly different among the different classes ($p < 0.001$, pairwise test with *Tukey–Kramer* adjacent), except between classes I and II ($p = 0.06$) [Figure 5b]. The $\delta^{15}N_{POM}$ values were significantly different among the different classes ($p < 0.001$, pairwise test with *Tukey–Kramer* adjacent), except between classes III and IV ($p = 0.76$) [Figure 5c]. However, the mean ± SD values of $\delta^{15}N_{POM}$ in classes III and IV were within the range of class II values [Figure 5c]. Therefore, the characteristics of $\delta^{13}C_{POM}$ and $\delta^{15}N_{POM}$ in classes I, II, III, and IV were middle-$\delta^{13}C_{POM}$ and low-$\delta^{15}N_{POM}$, middle-$\delta^{13}C_{POM}$ and high-$\delta^{15}N_{POM}$, low-$\delta^{13}C_{POM}$ and high-$\delta^{15}N_{POM}$, and high-$\delta^{13}C_{POM}$ and high-$\delta^{15}N_{POM}$, respectively.

Environmental conditions (temperature, salinity, nitrate concentration, chlorophyll-*a* concentration, and C:N ratio) differed significantly among the classes (ANOVA, $p < 0.01$; Figure 6). The temperature was lower in class I (mean ± SD: 10.1 ± 2.0°C) and III (12.7 ± 6.0°C) than in classes II (20.1 ± 4.9°C) and IV (24.0 ± 2.6°C) [Figure 6a]. Significant differences in temperature were discerned ($p < 0.003$, pairwise test with *Tukey–Kramer* adjacent) among different classes, except between classes I and III ($p = 0.44$). The only significant difference in salinity among the classes was discerned between classes II (33.76 ± 0.79) and III (34.27 ± 0.18) ($p = 0.01$, pairwise test with *Tukey–Kramer* adjacent) [Figure 6b]. The mean salinity with SD of classes I and IV were 33.99 ± 0.06 and 33.91 ± 0.36, respectively [Figure 6b]. The mean nitrate concentration values were high in classes I (4.20 ± 1.31 µM) and III (3.88 ± 3.86 µM), lower in class II (0.51 ± 1.31 µM), and the lowest in class IV (0.05 ± 0.01 µM) [Figure 6c]. The chlorophyll-*a* concentrations were significantly different among the classes (ANOVA, degrees of freedom [DF] = 3, *F*-value = 2.643, $p = 0.048$). However, no significant differences were identified among the pairs ($p > 0.058$). In particular, the chlorophyll-*a* concentration was the highest in class IV (0.69 ± 1.33 µg L^{-1}), followed by class I (0.61 ± 0.23 µg L^{-1}), class III (0.58 ± 0.37 µg L^{-1}), and the lowest in class II (0.44 ± 0.48 µg L^{-1}) [Figure 6d]. Moreover, a high C:N ratio was identified in class IV (7.06 ± 1.50 mol mol^{-1}), which was significantly higher ($p < 0.01$, pairwise test with *Tukey–Kramer* adjacent) than in classes II (6.13 ± 1.39 mol mol^{-1}) and III (5.12 ± 1.22 mol mol^{-1}). However, the C:N ratio in class IV did not differ from that in class I (6.05 ± 0.58 mol mol^{-1}) [Figure 6e].

The T–S diagram demonstrated that the samples of class I were mostly (10 of 11 samples) in the water with the temperature and salinity within the 9.4–11.4°C and 33.877–34.038 ranges, respectively [Figure 7a]. Only a single sample of class I was identified at a temperature and salinity of 4.3°C and 34.037, respectively, in April [Figure 7a]. The one sample classified as class II was identified in April in the surface layer, with the temperature and salinity ranging from 9.4–11.4°C and < 34.038, respectively. The nitrate concentration, $\delta^{13}C_{POM,}$ and $\delta^{15}N_{POM}$ of this sample were 0.28 µM, –25.3‰, and 3.5‰, respectively. However, in the N-σ_t diagram, the samples were not characterized according to the classes [Figure 7b].

3.5 Relationships with environmental conditions

According to the GMM, both $\delta^{13}C_{POM,}$ and $\delta^{15}N_{POM}$ exhibited multi-modal distribution. The linear regression was based on the assumption that the dependent variable has a normal distribution; therefore, in this study, the linear regressions were inappropriate for evaluating the relationships. We have provided the results of the linear regression analysis in the supporting information.

The least AIC GLM for $\delta^{13}C_{POM}$ was as follows:

$$\delta^{13}C_{POM} \sim \text{glm}[f(\text{class}) + f(\text{layer}) + \text{Lat} + \text{T} + \text{S} + \text{Chl} + \text{Nitrate}] \quad (3).$$

The r^2 value of the least AIC $\delta^{13}C_{POM}$ model was found to be 0.659. ANOVA indicated that all the remaining explanatory variables were significant ($\chi^2 \geq 7.53$, $p \leq 0.006$). The responses of latitude, salinity, and nitrate concentration were significantly negative ($p < 0.001$), whereas those of temperature and chlorophyll-*a* concentration were significantly positive ($p < 0.001$) [Figure 8]. The lsmean $\delta^{13}C_{POM}$ with ANOVA suggested that classes III (lsmean ± SE: –25.6 ± 0.25‰) and IV (–20.6 ± 0.19‰) were significantly higher and lower than those of other classes, respectively (pair-wise test with Tukey's adjacent, $p < 0.001$). The difference between classes I (–23.0 ± 0.36‰) and II (–23.4 ± 0.10‰) was insignificant (pair-wise test with Tukey's adjacent, $p = 0.542$) [Figure 8a]. The $\delta^{13}C_{POM}$ of the surface (lsmean ± SE: –23.4 ± 0.11‰) was higher than that of the subsurface (–23.7 ± 0.13‰, pair-wise test with Tukey's adjacent, $p = 0.0154$). Moreover, $\delta^{13}C_{POM}$ at the 100-m depth (–22.4 ± 0.34‰) was significantly higher than those of the surface and subsurface ($p \leq 0.001$) [Figure 8].

The least-AIC $\delta^{15}N_{POM}$ GLM was as follows:

$$\delta^{15}N_{POM} \sim \text{glm}[f(\text{class}) + f(\text{season}) + f(\text{layer}) + \text{Lon} + \text{Lat} + \text{T} + \text{S}] \quad (4).$$

All the parameters were statistically significant (ANOVA, $p < 0.001$), and the r^2 value of the model was found to be 0.451. The longitude had a positive impact on $\delta^{15}N_{POM}$, i.e., $\delta^{15}N_{POM}$ increased eastward [Figure 9e]. The $\delta^{15}N_{POM}$ was negatively affected by the latitude, temperature, and salinity [Figure 9d, f, g]. The lsmean values indicated that the $\delta^{15}N_{POM}$ of classes I (lsmean ± SE: –1.6 ± 0.41‰) and II (–3.1 ± 0.22‰) were significantly lower and higher than those of the other three classes, respectively (pair-wise test with Tukey's adjacent, $p < 0.01$). Moreover, classes III (2.1 ± 0.34‰) and IV (2.0 ± 0.29‰) were not significantly different ($p = 0.9735$). The seasonal variations exhibited significant differences between spring (1.3 ± 0.25‰) and summer (1.9 ± 0.18‰, pair-wise test with Tukey's adjacent, $p < 0.01$), while the lowest lsmean values were recorded in winter (0.9 ± 0.43‰). No significant differences of lsmean $\delta^{15}N_{POM}$ were found between spring and summer ($p > 0.0897$). The layer indicated that $\delta^{15}N_{POM}$ at a depth of 100 m (2.3 ± 0.39‰) was significantly higher (pair-wise test with Tukey's adjacent, $p < 0.01$) than that at the surface (0.9 ± 0.15‰) and subsurface (1.0 ± 0.21‰).

4. Discussion

This study, for the first time, revealed $\delta^{13}C_{POM}$ and $\delta^{15}N_{POM}$ in a wide area of the southern SOJ. Previous studies on $\delta^{13}C_{POM}$ and $\delta^{15}N_{POM}$ were confined to the coastal areas of the southern SOJ [*Antonio et al.*, 2012; *Nakamura et al.*, 2022] and sinking particles [*Nakanishi and Minagawa*, 2003]. Seasonality was demonstrated by the $\delta^{13}C$ and $\delta^{15}N$ values of sinking organic particles in the deep layer (> 500 m depth) [*Nakanishi and Minagawa*, 2003]. Significant seasonality of $\delta^{13}C_{POM}$ and $\delta^{15}N_{POM}$ was observed on the surface in our study, although the pattern of $\delta^{13}C$ differed from that seen by *Nakanishi and Minagawa* [2003]. In *Nakanishi and Minagawa* [2003], the $\delta^{13}C$ of sinking particles increased with bloom period. However, in our study, the $\delta^{13}C_{POM}$ decreased along the SI-line. On the contrary, the seasonality of $\delta^{15}N$ of the sinking particles and $\delta^{15}N_{POM}$ was comparable. We were unable to determine why the seasonality of $\delta^{13}C_{POM}$ of our study differed from that of *Nakanishi and Minagawa* [2003]. However, our observations indicated that the $\delta^{13}C_{POM}$ and $\delta^{15}N_{POM}$ values at 100-m depth, below the euphotic layer, were significantly different from those in the euphotic zone [Figure 2], and monthly variations were not significant below the mixed layer. Thus, the characteristics of the sinking particles in the SOJ may be different from those of POM in the surface layer.

4.1. Variations and the causes of carbon isotope ratio

According to the GLM approach, environmental characteristics may explain approximately two-thirds of the variations in $\delta^{13}C_{POM}$. The relationships found in this study are consistent with previous observations. When environmental conditions were ignored, seasonal variation was significant; nevertheless, seasonal variation was not selected as an explanatory variable in the GLM, suggesting that environmental parameters can well explain the seasonality of $\delta^{13}C_{POM}$. The positive associations observed between temperature or chlorophyll-*a* concentration and $\delta^{13}C_{POM}$ were similar to those observed in earlier ocean and incubation experiments [*Fontugne and Duplessy*, 1981; *Goericke and Fry*, 1994; *Miller et al.*, 2013; *Savoye et al.*, 2003]. Phytoplankton community growth rates are probably high in the warm water [*Sherman et al.*, 2016], and high chlorophyll-*a* concentrations are considered to be a consequence of rapid phytoplankton growth. During the rapid growth phase, phytoplankton utilizes more $^{13}CO_2$ utilization in the water, consequently elevating $\delta^{13}C_{POM}$ [*Freeman and Hayes*, 1992].

The negative relationship between $\delta^{13}C_{POM}$ and salinity or nitrate concentration has been previously reported in Kuroshio and western North Pacific boundary currents [*Kodama et al.*, 2021]. The negative relationship between salinity in the Kuroshio area was considered to be a mixture of POM formed in the estuary [*Kodama et al.*, 2021], where phytoplankton bloom occurs and then high $\delta^{13}C_{POM}$ POM are formed [*Ogawa and Ogura*, 1997; *Savoye et al.*, 2003]. Additionally, the elevated $\delta^{13}C_{POM}$ may be due to sediment resuspension in the Changjiang estuary [*Gao et al.*, 2014]. Although our samples were occasionally obtained near Japanese coastal regions, the less saline water of this sea is mostly due to the influence of the East China Sea [*Kosugi et al.*, 2021]. In the East China Sea, $\delta^{13}C_{POM}$ is negatively associated with salinity [*Ho et al.*, 2021], and high $\delta^{13}C_{POM}$ (> –20‰) is detected in the Changjiang diluted waters [*Gao et al.*, 2014]. However, *Gao et al.* [2014] did not report the hydrographic characteristics in the high $\delta^{13}C_{POM}$ area, and thus, the relationship between salinity and $\delta^{13}C_{POM}$ was unknown. The direct influence of terrestrial organic matter from China may be ignored: the $\delta^{13}C_{POM}$ in the Changjiang river is < –25‰ [*Gao et al.*, 2014], while the contribution of terrestrial organic

matter is <10% 500 km away from the Changjiang estuary [*Wu et al.*, 2003]. The effects of Japanese local rivers cannot be ignored, where river-originated $\delta^{13}C_{POM}$ is ~ –24‰ and lower than the ocean-originated $\delta^{13}C_{POM}$ [*Antonio et al.*, 2012], and thus, the direct influence of terrestrial organic matter is deemed to be restricted in the SOJ based on the relationship between salinity and $\delta^{13}C_{POM}$. These results suggest that POM with high-$\delta^{13}C_{POM}$ from the less saline waters of the East China Sea is transported into the SOJ and influences the spatiotemporal variation of $\delta^{13}C_{POM}$ in the SOJ, particularly during the summer, when the Changjiang-origin freshwater inputs to the SOJ via the Tsushima Strati are the highest among the seasons [*Morimoto et al.*, 2009]. However, in the instance of the Delaware Estuary in the United States, high seasonality of $\delta^{13}C_{POM}$ (–17‰ in spring while –32‰ in summer) was reported [*Fogel et al.*, 1992], and it was a possibility that POM with low-$\delta^{13}C_{POM}$ was formed in both the Changjiang estuary and Delaware Estuary. Carbon assimilation and decomposition processes in the less-saline waters, which were not observed in this study, must thus be investigated in the future. We could not come up with a plausible explanation for the negative relationship between latitude and nitrate concentration.

The environmental parameters properly explained $\delta^{13}C_{POM}$ variability, but not the difference among classes (III and IV) because it was significant in the GLM. Temperature, nitrate concentration, and C:N ratio were found to be significantly different across classes III and IV. Furthermore, the class IV samples were mostly from the surface layer during the summer, but the surface layer samples during summer were not classified as the class III. *Nakatsuka et al.* [1992] reported that $\delta^{13}C_{POM}$ levels are high in the late phytoplankton bloom phase. Thus, the high $\delta^{13}C_{POM}$ with low nitrate concentration and high C:N ratio in the class IV samples may be attributed to active carbon assimilation under nitrate depletion conditions. However, because the chlorophyll *a* concentration was low in the class IV samples, additional processes must be considered. According to the T-S diagram, class IV POM was mainly collected in the warm and saline waters in 2019. This may indicate that the isotope fraction in this water is different; for example, an increase in diatom abundance elevates $\delta^{13}C_{POM}$ [*Lowe et al.*, 2014], but the diatom contribution in the SOJ is low during the summer [*Kodama et al.*, 2022b]. The phytoplankton community structure was not assessed in this study and will need to be investigated more in the future. In contrast to class IV samples, low $\delta^{13}C_{POM}$ samples in class III were mostly observed in nitrate-rich waters, indicating that primary production is not active, which might be due to light limitation and deep mixing; the previous study's iron limitation for primary production was rejected [*Fujita et al.*, 2010]. However, comparable environmental conditions of classes III and IV samples were observed in the classes I and II samples, and hence the fundamental reason why the $\delta^{13}C_{POM}$ was low and high in classes III and IV, respectively, is yet unclear.

4.2. Unique nitrogen dynamics in the SOJ

Unlike $\delta^{13}C_{POM}$, $\delta^{15}N_{POM}$ was not adequately explained by environmental parameters based on the detection coefficient values. Temperature and salinity remained as explanatory variables in the variation of $\delta^{15}N_{POM}$ in the ocean, but were not regarded as essential determinants [*Sigman et al.*, 2009]. Temperature had the opposite impact reported in the Kuroshio [*Kodama et al.*, 2021]. Temperature had no significant effect in the western south East China Sea [*Ho et al.*, 2021], thereby suggesting that the negative impact of temperature on the $\delta^{15}N_{POM}$ was specific to the SOJ; however, its mechanisms remain unclear.

The negative impact of salinity was similar to that observed in the Kuroshio [*Kodama et al.*, 2021]. In June 2010, the $\delta^{15}N_{POM}$ in the surface less-saline Changjiang diluted water (at 5 m depth and salinity <30) was recorded to be ~9‰ in the northern part of the East China Sea [*Sukigara et al.*, 2017]. In 2011, the $\delta^{15}N_{POM}$ in the Changjiang diluted water in 2011 was ~6‰ [*Sukigara et al.*, 2017]. *Sukigara et al.* [2017] stated that POM with high $\delta^{15}N_{POM}$ was not always present in the Changjiang diluted water, although high $\delta^{15}N_{POM}$ was also reported in the East China Sea in previous studies [*Gao et al.*, 2014; *Wu et al.*, 2003]. These findings corroborate the hypothesis that high $\delta^{15}N_{POM}$ levels originate from the less-saline Changjiang diluted water that mainly flows into the SOJ during the summer [*Morimoto et al.*, 2009], as well as the negative relationship between salinity and $\delta^{15}N_{POM}$.

There are two proposed mechanisms for the influence of latitude on the $\delta^{15}N_{POM}$. One is the Japanese territorial influence. The other is the impact of the coastal branch of the Tsushima Warm Current. The coastal branch of the Tsushima Warm Current originates from the eastern channel of the Tsushima Strait and flows along the Japanese coast [*Katoh*, 1994]. Our monitoring regions always included a coastal region in the low latitude area, as well as flows of the coastal branch of the Tsushima Warm Current [*Katoh*, 1994]. The $\delta^{13}C_{POM}$ did not indicate direct territorial inputs in this case, thus the influence of the coastal branch of the Tsushima Warm Current and the origin of the waters may be the explanation.

Although ocean observations indicated a negative relationship between $\delta^{15}N_{POM}$ and nitrate concentration based on Rayleigh fractionation [*Sigman et al.*, 2009] has been supported in the ocean observations [*Ho et al.*, 2021; *Kodama et al.*, 2021], the negative relationship in the SOJ remained equivocal. Even in an open system, kinetic isotope effects ($\delta^{15}N$ difference between reactant and product) and the degree of consumption of reactant theoretically determine the $\delta^{15}N$ value of the product, and when the remaining reactant is zero (i.e., completely consumed), the $\delta^{15}N$ of a product is equal to the original $\delta^{15}N$ of reactant [*Sigman et al.*, 2009]. In this case, the kinetic isotope effect of nitrate on POM is ~3‰ [*Sigman et al.*, 2009]. Thus, $\delta^{15}N_{POM}$ is theoretically 0–3‰ lower than $\delta^{15}N$ of nitrate ($\delta^{15}N_{NO3}$), and with nitrate consumption, it increases and approaches the original $\delta^{15}N_{NO3}$ value. The monthly variations in the surface layer along the SI-line indicated that the $\delta^{15}N_{POM}$ increases from winter to summer, and the GLM method confirms this trend. This also indicates that nitrate depletion partly contributes to the increase in $\delta^{15}N_{POM}$. Because $\delta^{15}N_{POM}$ was not normally distributed, the association was insignificant ($p = 0.4467$) when we removed class I POM, indicating that the relationships between $\delta^{15}N_{POM}$ and the environment, especially the nitrate concentration in the SOJ, were unique.

The following are three hypotheses for the ambiguous relationship between $\delta^{15}N_{POM}$ and nitrate concentration: (1) our dataset; and (2) the variety of nitrogen sources. First, our observations were mainly conducted in the summer, during which time the nitrate was depleted at the surface, and the nitrate concentration in 182 of the 494 samples was not detectable (< 0.01 μM). The $\delta^{15}N_{POM}$ in the nitrate-depleted waters varied greatly (mean ± SD: 2.8 ± 1.2‰, n = 182). This $\delta^{15}N_{POM}$ variation in nitrate-depleted water may have rendered the relationship between $\delta^{15}N_{POM}$ and nitrate concentration unclear, rendering the association statistically insignificant. When the GLM approach was conducted for subsamples with detectable nitrate (>0.01 μM), the nitrate concentration remained as the explanatory variable in the least-AIC model; the coefficient was negative but not significant (ANOVA, $p = 0.12$). As a result, the

imbalanced dataset was not rejected; nonetheless, it was not the primary cause of the ambiguous relationship between $\delta^{15}N_{POM}$ and nitrate concentration.

Second, the nitrogenous (nitrate) source of the SOJ exhibited variability. Previous studies in the Northern East China Sea [*Umezawa et al.*, 2021; *Umezawa et al.*, 2014] found four nitrate sources with varying $\delta^{15}N_{NO3}$. The nitrate with high-$\delta^{15}N_{NO3}$ (8.3‰) originated from the Changjiang freshwater in July, the nitrate with low-$\delta^{15}N_{NO3}$ (2.0‰) originated from the Changjiang estuary in July, the $\delta^{15}N_{NO3}$ in the water originating from the Kuroshio is 5.5–6.0‰ in February, and that originating from atmospheric deposition is -4–0‰ [*Umezawa et al.*, 2021; *Umezawa et al.*, 2014]. Furthermore, active nitrogen fixation occurs in the northwestern part of the East China Sea [*Shiozaki et al.*, 2010], and $\delta^{15}N_{POM}$ originating from nitrogen fixation is -2.1–0.8‰ [*Minagawa and Wada*, 1986]. According to these results, the $\delta^{15}N_{POM}$ formed by nitrate assimilation and nitrogen fixation exhibited a wider range. In fact, in the East China Sea, where the TWC originates, $\delta^{15}N_{POM}$ near the surface varies widely by about -5–9‰ during summer [*Gao et al.*, 2014] and 2–6‰ in autumn [*Wu et al.*, 2003]. Horizontal advective transport of nitrate from the East China Sea is the key factor for controlling primary production in the SOJ throughout the summer [*Kodama et al.*, 2017; *Kodama et al.*, 2015]. POM originating from diverse nitrogenous sources will be mixed during the horizontal advection processes in the TWC and the East China Sea, and POM from the East China Sea is expected to flow into the SOJ with nitrate. The numerous nitrogen source contributions would obscure the $\delta^{15}N_{POM}$ and nitrate concentration in the SOJ.

Here, *in-silico* simulation of the relationship between the $\delta^{15}N_{POM}$ and nitrate concentration was performed. The $\delta^{15}N_{NO3}$ was set to 0–8.3‰ [*Umezawa et al.*, 2021; *Umezawa et al.*, 2014], the kinetic isotope effects to 3‰ [*Sigman et al.*, 2009], and the supplied nitrate concentration to 0.05–5 μM. The $\delta^{15}N_{POM}$ was then calculated by mixing nitrate-origin POM and nitrogen-fixation-origin POM. Based on observations in the southern East China Sea in summer, the contribution of nitrogen fixation to nitrate assimilation in the water column was reported as 10–82% [*Liu et al.*, 2013].The contribution of nitrogen fixation to the primary production in *Liu et al.* [2013] (1.9–5.8%) was comparable to that of the SOJ in June (~3.8%) [*Sato et al.*, 2021]. Therefore, the contribution of nitrogen fixation to $\delta^{15}N_{POM}$ was set at 10–82% [*Liu et al.*, 2013]. $\delta^{15}N_{POM}$ produced with nitrogen fixation was set at -2.1–0.8‰ [*Minagawa and Wada*, 1986]. Assuming that the parameters and fraction of remanent nitrate (0–100%), except kinetic isotope effects, were randomly varied in this simulation, and the sample size was set to 500, the insignificant relationship between the $\delta^{15}N_{POM}$ and nitrate concentration was observed in ~30% of the simulations (replicated 1000 times). On the other hand, when the $\delta^{15}N_{NO3}$ was adjusted to 5–6‰, the significant negative relationship between $\delta^{15}N_{POM}$ and nitrate concentration was consistently observed. This result supports our hypothesis that the relationship between the $\delta^{15}N_{POM}$ and nitrate concentration is disrupted by the numerous nitrogen sources.

Another distinctive feature of the SOJ was the low-$\delta^{15}N_{POM}$ designated class I, which was found in the winter and spring, and is characterized in the T-S diagrams. The low-$\delta^{15}N_{POM}$ was mainly observed in temperature and salinity ranges of 9.4–11.4°C and 33.877–34.038, respectively. *Wagawa et al.* [2020] classified this water as "upper low salinity water" (ULSW). Despite the fact that the origin of USLW was unclear, *Wagawa et al.* [2020] proposed that it originated from Toyama Bay, with a less saline condition caused by the mixing with local Japanese rivers. It is reasonable to assume that the USLW is not mixed with the saline TWC water (its salinity is ~ 34.5). Because this saline TWC water originates from the Kuroshio

Current, the $\delta^{15}N_{NO3}$ of the saline TWC water is estimated to be 5.5–6.0‰ in accordance with *Umezawa et al.* [2014]. At the same time, the $\delta^{15}N_{NO3}$ of local Japanese rivers has been estimated to be 0–2‰ [*Sugimoto et al.*, 2019], suggesting that the POM in the ULSW may have originated from lower $\delta^{15}N_{NO3}$-nitrate than the Kuroshio-origin nitrate, and hence the $\delta^{15}N_{POM}$ is lower than the other water masses. The horizontal distribution of ULSW is not reported, but we assumed that it was not large and confined to winter and spring based on *Wagawa et al.* [2020], hence the low-$\delta^{15}N_{POM}$ area would be limited to season and area. Phytoplankton bloom is another possibility for class I. $\delta^{15}N_{POM}$ rapidly declined at the start of the phytoplankton bloom phase but quickly rose with nitrate depletion [*Nakatsuka et al.*, 1992]. However, we believe that such scenario is uncommon and did not have a significant impact on our observations because the majority of class I samples were collected in February, and the phytoplankton bloom occurred at the end of March [*Kodama et al.*, 2018; *Maúre et al.*, 2017].

Seasonality remained significant after accounting for hydrographic conditions in the GLM. Not only nitrate concentrations but also nitrogen sources have a seasonality in the SOJ. The mixed layer deepens in the winter, and hence the nitrate originated in deep-sea water or local Japanese rivers in this season. The utilization of nitrate provided in winter occurs in spring, and the Tsushima Warm Current remains weak [*Yabe et al.*, 2021]. *Kodama et al.* [2015] also showed that subsurface nutrient maximum induced by the horizontal advective transport of the Tsushima Warm Current could be observed from the beginning of June. Therefore, the seasonality of $\delta^{15}N_{POM}$ may be associated with horizontal advective transport, albeit additional research is required to understand the seasonality.

We identified the interannual variations in $\delta^{13}C_{POM}$ and $\delta^{15}N_{POM}$ during summer using repetitive measurements along the SI-line. In 2019, low $\delta^{15}N_{POM}$ with high $\delta^{13}C_{POM}$ was observed compared to that in 2018, despite the fact that the environmental conditions were not significantly different among these four years (2016, 2018–2020). These interannual variations may be influenced by horizontal advection. We were unable to gather data on the contribution of the horizontal advection processes, however, interannual variations in salinity and phosphate concentration in the East China Sea are linked to those of SOJ [*Kodama et al.*, 2016; *Kosugi et al.*, 2021]. In the East China Sea, the interannual difference in $\delta^{15}N_{POM}$ in the Changjiang diluted water was reported by *Sukigara et al.* [2017] and *Ho et al.* [2021] revealed an interannual difference in $\delta^{15}N_{POM}$ in the Changjiang diluted water in the East China Sea, which may influence $\delta^{13}C_{POM}$ and $\delta^{15}N_{POM}$ in the SOJ. The causes of interannual variations are not described by *Sukigara et al.* [2017] or *Ho et al.* [2021], and we were unable to determine them in our study.

5. Conclusions

In this study, the $\delta^{13}C_{POM}$ and $\delta^{15}N_{POM}$ values in the southern SOJ were investigated and reported for the first time. Our observations were mostly conducted in the summer, therefore our identified characteristics of $\delta^{13}C_{POM}$ and $\delta^{15}N_{POM}$ mainly reflected the characteristics of the summer of SOJ, while seasonality, except autumn, was covered by the monitoring line. There were significant seasonal variations in $\delta^{13}C_{POM}$ and $\delta^{15}N_{POM}$ in the surface mixed layer, but not below the mixed layer (at 30 m depth). Environmental variables and primary production processes adequately explained the observed $\delta^{13}C_{POM}$ value. $\delta^{13}C_{POM}$ could be estimated using our GLM and routine hydrographic observations. However, environmental variables did not adequately explain the variation in $\delta^{15}N_{POM}$. In particular, the relationship between nitrate

concentration was not found. The SJO contains different nitrogenous sources, such as atmospheric depositions and riverine inputs, and $\delta^{15}N_{POM}$ indicates that these sources are mixed and support primary production. The *in-silico* simulation supported that multiple nitrate sources contributed to the ambiguous relationship between $\delta^{15}N_{POM}$ and nitrate concentration. The main nitrogen source in the SOJ was not detected in our study, but the new production was dependent on the nitrate supplied from these sources. Anthropogenic nitrogen inputs were increased in the SOJ [*Duan et al.*, 2007; *Kitayama et al.*, 2012], and hence, the new production in the SOJ is expected to increase. As a result, we must evaluate the impact of "increased" new production on the biogeochemical cycles and ecosystems in the SOJ.

Acknowledgments

We would like to thank the captains, crews, researchers, and staff who took part in the cruises. We state that there is no conflict of interest, and the Japanese government granted authorization for all of observations in accordance with the Japanese legislation. This work has been funded by a research and assessment program for fisheries resources from the Fisheries Agency of Japan, grants from the Japan Fisheries Research and Education Agency, and Japan Society for the Promotion of Science grants for Taketoshi Kodama, Yosuke Igeta, and Yoichi Kogure (19K06198).

Open Research

The stable isotope ratio of POM with environmental data used for the statistical analysis in the study is available at PANGAEA (https://doi.org/10.1594/PANGAEA.949287).

References

Antonio, E. S., A. Kasai, M. Ueno, Y. Ishihi, H. Yokoyama, and Y. Yamashita (2012), Spatial-temporal feeding dynamics of benthic communities in an estuary-marine gradient, *Estuar. Coast. Shelf Sci.*, *112*, 86-97, doi:10.1016/j.ecss.2011.11.017.

Buchanan, P. J., R. J. Matear, Z. Chase, S. J. Phipps, and N. L. Bindoff (2019), Ocean carbon and nitrogen isotopes in CSIRO Mk3L-COAL version 1.0: a tool for palaeoceanographic research, *Geosci. Model Dev.*, *12*(4), 1491-1523, doi:10.5194/gmd-12-1491-2019.

Duan, S. W., F. Xu, and L. J. Wang (2007), Long-term changes in nutrient concentrations of the Changjiang River and principal tributaries, *Biogeochemistry*, *85*(2), 215-234, doi:10.1007/s10533-007-9130-2.

Fogel, M. L., L. A. Cifuentes, D. J. Velinsky, and J. H. Sharp (1992), Relationship of carbon availability in estuarine phytoplankton to isotopic composition, *Mar. Ecol. Prog. Ser.*, *82*(3), 291-300.

Fontugne, M., and J. Duplessy (1981), Organic-carbon isotopic fractionation by marine plankton in the temperature range -1 to 31°C, *Oceanol. Acta*, *4*(1), 85-90.

Fox, J., and S. Weisberg (2018), *An R companion to applied regression*, Sage publications.

Freeman, K. H., and J. M. Hayes (1992), Fractionation of carbon isotopes by phytoplankton and estimates of ancient CO2 levels, *Global Biogeochem. Cycles*, *6*(2), 185-198, doi:10.1029/92GB00190.

Fujita, S., K. Kuma, S. Ishikawa, S. Nishimura, Y. Nakayama, S. Ushizaka, Y. Isoda, S. Otosaka, and T. Aramaki (2010), Iron distributions in the water column of the Japan Basin and Yamato Basin (Japan Sea), *J. Geophys. Res. Oceans*, *115*(C12), doi:10.1029/2010JC006123.

Gao, L., D. Li, and J. Ishizaka (2014), Stable isotope ratios of carbon and nitrogen in suspended organic matter: Seasonal and spatial dynamics along the Changjiang (Yangtze River) transport pathway, *Journal of Geophysical Research: Biogeosciences*, *119*(8), 1717-1737, doi:10.1002/2013JG002487.

Goericke, R., and B. Fry (1994), Variations of marine plankton $\delta^{13}C$ with latitude, temperature, and dissolved CO_2 in the world ocean, *Global Biogeochem. Cycles*, *8*(1), 85-90, doi:10.1029/93gb03272.

Gruber, N., and J. N. Galloway (2008), An Earth-system perspective of the global nitrogen cycle, *Nature*, *451*(7176), 293-296, doi:10.1038/nature06592.

631 Gruber, N., C. D. Keeling, R. B. Bacastow, P. R. Guenther, T. J. Lueker, M. Wahlen, H. A. J. Meijer, W. G. Mook,
632 and T. F. Stocker (1999), Spatiotemporal patterns of carbon-13 in the global surface oceans and the oceanic
633 suess effect, *Global Biogeochem. Cycles*, *13*(2), 307-335, doi:10.1029/1999gb900019.
634 Guo, X., Y. Miyazawa, and T. Yamagata (2006), The Kuroshio onshore intrusion along the shelf break of the East
635 China Sea: the origin of the Tsushima Warm Current, *J. Phys. Oceanogr.*, *36*(12), 2205-2231,
636 doi:10.1175/jpo2976.1.
637 Hashimoto, R., T. Yoshida, S. Kuno, T. Nishikawa, and Y. Sako (2012), The first assessment of cyanobacterial and
638 diazotrophic diversities in the Japan Sea, *Fish. Sci.*, *78*(6), 1293-1300, doi:10.1007/s12562-012-0548-7.
639 Ho, P.-C., N. Okuda, C.-F. Yeh, P.-L. Wang, G.-C. Gong, and C.-H. Hsieh (2021), Carbon and nitrogen isoscape of
640 particulate organic matter in the East China Sea, *Prog. Oceanogr.*, *197*, 102667,
641 doi:10.1016/j.pocean.2021.102667.
642 Ishizu, M., Y. Miyazawa, T. Tsunoda, and T. Ono (2019), Long-term trends in pH in Japanese coastal seawater,
643 *Biogeosciences*, *16*(24), 4747-4763, doi:10.5194/bg-16-4747-2019.
644 Isobe, A. (1999), On the origin of the Tsushima Warm Current and its seasonality, *Cont. Shelf Res.*, *19*(1), 117-133,
645 doi:10.1016/s0278-4343(98)00065-x.
646 Katoh, O. (1994), Structure of the Tsushima Current in the southwestern Japan Sea, *J. Oceanogr.*, *50*(3), 317-338.
647 Kim, S. K., K. I. Chang, B. Kim, and Y. K. Cho (2013), Contribution of ocean current to the increase in N
648 abundance in the Northwestern Pacific marginal seas, *Geophys. Res. Lett.*, *40*(1), 143-148,
649 doi:10.1029/2012GL054545.
650 Kim, T. W., K. Lee, R. G. Najjar, H. D. Jeong, and H. J. Jeong (2011), Increasing N abundance in the northwestern
651 Pacific Ocean due to atmospheric nitrogen deposition, *Science*, *334*(6055), 505-509,
652 doi:10.1126/science.1206583.
653 Kitayama, K., S. Seto, M. Sato, and H. Hara (2012), Increases of wet deposition at remote sites in Japan from 1991
654 to 2009, *Journal of Atmospheric Chemistry*, *69*(1), 33-46, doi:10.1007/s10874-012-9228-3.
655 Kodama, T. (2020), The nutrient dynamics and the lower trophic ecosystems in the warm waters in the vicinity of
656 Japan, *Oceanography in Japan*, *29*(2), 55-69, doi:10.5928/kaiyou.29.2_55.
657 Kodama, T., Y. Igeta, and N. Iguchi (2022a), Long-term variation in mesozooplankton biomass caused by top-down
658 effects: a case study in the coastal Sea of Japan, *Geophys. Res. Lett.*, *49*(15), e2022GL099037,
659 doi:10.1029/2022gl099037.
660 Kodama, T., Y. Igeta, M. Kuga, and S. Abe (2016), Long-term decrease in phosphate concentrations in the surface
661 layer of the southern Japan Sea, *J. Geophys. Res.*, *121*(10), 7845-7856, doi:10.1002/2016jc012168.
662 Kodama, T., A. Morimoto, T. Takikawa, M. Ito, Y. Igeta, S. Abe, K. Fukudome, N. Honda, and O. Katoh (2017),
663 Presence of high nitrate to phosphate ratio subsurface water in the Tsushima Strait during summer, *J.*
664 *Oceanogr.*, *73*(6), 759-769, doi:10.1007/s10872-017-0430-4.
665 Kodama, T., H. Morimoto, Y. Igeta, and T. Ichikawa (2015), Macroscale-wide nutrient inversions in the subsurface
666 layer of the Japan Sea during summer, *J. Geophys. Res.*, *120*(11), 7476-7492, doi:10.1002/2015jc010845.
667 Kodama, T., A. Nishimoto, S. Horii, D. Ito, T. Yamaguchi, K. Hidaka, T. Setou, and T. Ono (2021), Spatial and
668 seasonal variations of stable isotope ratios of particulate organic carbon and nitrogen in the surface water of
669 the Kuroshio, *J. Geophys. Res.*, *126*(4), e2021JC017175, doi:10.1029/2021JC017175.
670 Kodama, T., Y. Taniuchi, H. Kasai, T. Yamaguchi, M. Nakae, and Y. Okumura (2022b), Empirical estimation of
671 marine phytoplankton assemblages in coastal and offshore areas using an in situ multi-wavelength
672 excitation fluorometer, *PLOS ONE*, *17*(2), e0257258, doi:10.1371/journal.pone.0257258.
673 Kodama, T., T. Wagawa, S. Ohshimo, H. Morimoto, N. Iguchi, K. I. Fukudome, T. Goto, M. Takahashi, and T.
674 Yasuda (2018), Improvement in recruitment of Japanese sardine with delays of the spring phytoplankton
675 bloom in the Sea of Japan, *Fish. Oceanogr.*, *27*(4), 289-301, doi:10.1111/fog.12252.
676 Kosugi, N., N. Hirose, T. Toyoda, and M. Ishii (2021), Rapid freshening of Japan Sea Intermediate Water in the
677 2010s, *J. Oceanogr.*, *77*(2), 269-281, doi:10.1007/s10872-020-00570-6.
678 Kosugi, N., D. Sasano, M. Ishii, K. Enyo, and S. Saito (2016), Autumn CO_2 chemistry in the Japan Sea and the
679 impact of discharges from the Changjiang River, *J. Geophys. Res.*, *121*(8), 6536-6549,
680 doi:10.1002/2016jc011838.
681 Liu, X., K. Furuya, T. Shiozaki, T. Masuda, T. Kodama, M. Sato, H. Kaneko, M. Nagasawa, and I. Yasuda (2013),
682 Variability in nitrogen sources for new production in the vicinity of the shelf edge of the East China Sea in
683 summer, *Cont. Shelf Res.*, *61-62*, 23-30, doi:10.1016/j.csr.2013.04.014.
684 Lorrain, A., et al. (2020), Trends in tuna carbon isotopes suggest global changes in pelagic phytoplankton
685 communities, *Global Change Biolology*, *26*(2), 458-470, doi:10.1111/gcb.14858.

686 Lorrain, A., N. Savoye, L. Chauvaud, Y.-M. Paulet, and N. Naulet (2003), Decarbonation and preservation method
687 for the analysis of organic C and N contents and stable isotope ratios of low-carbonated suspended
688 particulate material, *Analytica Chimica Acta*, *491*(2), 125-133, doi:10.1016/S0003-2670(03)00815-8.
689 Lowe, A. T., A. W. E. Galloway, J. S. Yeung, M. N. Dethier, and D. O. Duggins (2014), Broad sampling and
690 diverse biomarkers allow characterization of nearshore particulate organic matter, *Oikos*, *123*(11), 1341-
691 1354, doi:10.1111/oik.01392.
692 Lüdecke, D. (2018), ggeffects: Tidy Data Frames of Marginal Effects from Regression Models, *Journal of Open*
693 *Source Software*, *3*(26), 772, doi:10.21105/joss.00772.
694 Maúre, E. R., J. Ishizaka, C. Sukigara, Y. Mino, H. Aiki, T. Matsuno, H. Tomita, J. I. Goes, and H. R. Gomes
695 (2017), Mesoscale eddies control the timing of spring phytoplankton blooms: A case study in the Japan
696 Sea, *Geophys. Res. Lett.*, *44*(21), 11,115-111,124, doi:10.1002/2017GL074359.
697 Miller, R. J., H. M. Page, and M. A. Brzezinski (2013), δ13C and δ15N of particulate organic matter in the Santa
698 Barbara Channel: drivers and implications for trophic inference, *Mar. Ecol. Prog. Ser.*, *474*, 53-66,
699 doi:10.3354/meps10098.
700 Minagawa, M., and E. Wada (1986), Nitrogen isotope ratios of red tide organisms in the East China Sea: A
701 characterization of biological nitrogen fixation, *Mar. Chem.*, *19*(3), 245-259, doi:10.1016/0304-
702 4203(86)90026-5.
703 Morimoto, A., T. Takikawa, G. Onitsuka, A. Watanabe, M. Moku, and T. Yanagi (2009), Seasonal variation of
704 horizontal material transport through the eastern channel of the Tsushima Straits, *J. Oceanogr.*, *65*(1), 61-
705 71, doi:10.1007/s10872-009-0006-z.
706 Nakamura, K., A. Nishimoto, S. Yasui-Tamura, Y. Kogure, M. Nakae, N. Iguchi, H. Morimoto, and T. Kodama
707 (2022), Carbon and nitrogen dynamics in the coastal Sea of Japan inferred from 15 years of measurements
708 of stable isotope ratios of *Calanus sinicus*, *Ocean Sci.*, *18*(2), 295-305, doi:10.5194/os-18-295-2022.
709 Nakanishi, T., and M. Minagawa (2003), Stable carbon and nitrogen isotopic compositions of sinking particles in the
710 northeast Japan Sea, *Geochem. J.*, *37*(2), 261-275, doi:10.2343/geochemj.37.261.
711 Nakatsuka, T., N. Handa, E. Wada, and C. S. Wong (1992), The dynamic changes of stable isotopic ratios of carbon
712 and nitrogen in suspended and sedimented particulate organic matter during a phytoplankton bloom, *J.*
713 *Mar. Res.*, *50*(2), 267-296, doi:10.1357/002224092784797692.
714 Ogawa, N., and N. Ogura (1997), Dynamics of particulate organic matter in the Tamagawa estuary and inner Tokyo
715 Bay, *Estuar. Coast. Shelf Sci.*, *44*(3), 263-273, doi:10.1006/ecss.1996.0118.
716 Ohishi, S., H. Aiki, T. Tozuka, and M. F. Cronin (2019), Frontolysis by surface heat flux in the eastern Japan Sea:
717 importance of mixed layer depth, *J. Oceanogr.*, *75*(3), 283-297, doi:10.1007/s10872-018-0502-0.
718 Ohshimo, S., T. Kodama, T. Yasuda, S. Kitajima, T. Tsuji, H. Kidokoro, and H. Tanaka (2021), Potential fluctuation
719 of δ13C and δ15N values of small pelagic forage fish in the Sea of Japan and East China Sea, *Mar.*
720 *Freshwater Res.*, *72*(12), 1811, doi:10.1071/mf20351.
721 Omstedt, A. (2021), How to develop an understanding of the marginal sea system by connecting natural and human
722 sciences, *Oceanologia*, doi:10.1016/j.oceano.2021.06.003.
723 Ono, T. (2021), Long-term trends of oxygen concentration in the waters in bank and shelves of the Southern Japan
724 Sea, *J. Oceanogr.*, *77*(4), 659-684, doi:10.1007/s10872-021-00599-1.
725 R Core Team (2023), R: A language and environment for statistical computing, edited by R Foundation for
726 Statistical Computing, https://www.R-project.org/. Vienna, Austria.
727 Ren, H., Y. C. Chen, X. T. Wang, G. T. F. Wong, A. L. Cohen, T. M. DeCarlo, M. A. Weigand, H. S. Mii, and D.
728 M. Sigman (2017), 21st-century rise in anthropogenic nitrogen deposition on a remote coral reef, *Science*,
729 *356*(6339), 749-752, doi:10.1126/science.aal3869.
730 Sato, T., T. Shiozaki, Y. Taniuchi, H. Kasai, and K. Takahashi (2021), Nitrogen Fixation and Diazotroph
731 Community in the Subarctic Sea of Japan and Sea of Okhotsk, *J. Geophys. Res. Oceans*, *126*(4),
732 e2020JC017071, doi:10.1029/2020jc017071.
733 Savoye, N., A. Aminot, P. Tréguer, M. Fontugne, N. Naulet, and R. Kérouel (2003), Dynamics of particulate
734 organic matter δ15N and δ13C during spring phytoplankton blooms in a macrotidal ecosystem (Bay of
735 Seine, France), *Mar. Ecol. Prog. Ser.*, *255*, 27-41, doi:10.3354/meps255027.
736 Scrucca, L., M. Fop, T. B. Murphy, and A. E. Raftery (2016), mclust 5: Clustering, classification and density
737 estimation using Gaussian finite mixture models, *The R journal*, *8*(1), 289-317, doi:10.32614/RJ-2016-021.
738 Sherman, E., J. K. Moore, F. Primeau, and D. Tanouye (2016), Temperature influence on phytoplankton community
739 growth rates, *Global Biogeochem. Cycles*, *30*(4), 550-559, doi:10.1002/2015gb005272.

Shiozaki, T., K. Furuya, T. Kodama, S. Kitajima, S. Takeda, T. Takemura, and J. Kanda (2010), New estimation of N2 fixation in the western and central Pacific Ocean and its marginal seas, *Global Biogeochem. Cycles*, *24*(1), GB1015, doi:10.1029/2009gb003620.

Sigman, D. M., K. L. Karsh, and K. L. Casciotti (2009), Nitrogen isotopes in the ocean, in *Encyclopedia of Ocean Sciences*, edited by J. H. Steele, pp. 40-54, Academic Press, Oxford, doi:10.1016/b978-012374473-9.00632-9.

Sugimoto, R., T. Tsuboi, and M. S. Fujita (2019), Comprehensive and quantitative assessment of nitrate dynamics in two contrasting forested basins along the Sea of Japan using dual isotopes of nitrate, *Sci. Total Environ.*, *687*, 667-678, doi:10.1016/j.scitotenv.2019.06.090.

Sukigara, C., Y. Mino, S. C. Tripathy, J. Ishizaka, and T. Matsuno (2017), Impacts of the Changjiang diluted water on sinking processes of particulate organic matters in the East China Sea, *Cont. Shelf Res.*, *151*, 84-93, doi:10.1016/j.csr.2017.10.012.

Umezawa, Y., K. Toyoshima, Y. Saitoh, S. Takeda, K. Tamura, C. Tamaya, A. Yamaguchi, C. Yoshimizu, I. Tayasu, and K. Kawamoto (2021), Evaluation of origin-depended nitrogen input through atmospheric deposition and its effect on primary production in coastal areas of western Kyusyu, Japan, *Environ. Pollut.*, *291*, 118034, doi:10.1016/j.envpol.2021.118034.

Umezawa, Y., A. Yamaguchi, J. Ishizaka, T. Hasegawa, C. Yoshimizu, I. Tayasu, H. Yoshimura, Y. Morii, T. Aoshima, and N. Yamawaki (2014), Seasonal shifts in the contributions of the Changjiang River and the Kuroshio Current to nitrate dynamics in the continental shelf of the northern East China Sea based on a nitrate dual isotopic composition approach, *Biogeosciences*, *11*(4), 1297-1317, doi:10.5194/bg-11-1297-2014.

Wagawa, T., Y. Kawaguchi, Y. Igeta, N. Honda, T. Okunishi, and I. Yabe (2020), Observations of oceanic fronts and water-mass properties in the central Japan Sea: Repeated surveys from an underwater glider, *J. Mar. Syst.*, *201*, 103242, doi:10.1016/j.jmarsys.2019.103242.

Wu, Y., J. Zhang, D. J. Li, H. Wei, and R. X. Lu (2003), Isotope variability of particulate organic matter at the PN section in the East China Sea, *Biogeochemistry*, *65*(1), 31-49, doi:10.1023/a:1026044324643.

Yabe, I., Y. Kawaguchi, T. Wagawa, and S. Fujio (2021), Anatomical study of Tsushima Warm Current system: Determination of Principal Pathways and its Variation, *Prog. Oceanogr.*, *194*, 102590, doi:10.1016/j.pocean.2021.102590.

Figure Captions

Figure 1. Map of the sampling stations. (a) Small-scale map of our observation area (break line square) with sea surface height and estimated ocean current positions (arrows: two offshore branches of Tsushima Warm Current, coastal branches of Tsushima Warm Current, and Kuroshio). (b) Sampling stations in winter (February), (c) in spring (March–June), and (d) in summer (July–September). The sea surface height was derived from Copernicus Marine Service Global Ocean Physics Reanalysis (GLORYS12V1, https://doi.org/10.48670/moi-00021) in August 2015. Along the SI-line [black solid line in (a) and gray line in (b) – (d)] set offshore of Sado Island, repeated observations were made. The crosses indicate the stations where samples were collected from the deep layer (75 m in spring and 100 m in summer), and open circles indicate stations where samples were collected only from the subsurface layer (20–65 m depth). In winter, all the sampling layers were assumed to be in the mixed layer, thus we did not divide them into surface and subsurface layers when collections were made at 10 m and 30 m depths.

Figure 2. The vertical profiles of (a) $\delta^{13}C_{POM}$, (b) $\delta^{15}N_{POM}$, and (c) the C:N ratio collected at nine stations in the eastern part of the Sea of Japan during September of 2020 (cross stations in Figure 1). Lines denote the profiles of every station. Box plots show the median (vertical thick lines within boxes), upper and lower quartiles (boxes), quartile deviations (horizontal bars), and outliers (closed circles).

Figure 3. Horizontal distributions of $\delta^{13}C_{POM}$ (upper, a–e) and $\delta^{15}N_{POM}$ (lower, f–j) in the Sea of Japan (1° × 1° grid median values for five years). The (a and f) winter, (b and g) in the surface layer of spring, (c and h) in the subsurface layer of spring, (d and i) in the surface layer of summer, and (e and j) in the subsurface layer of summer. Circle sizes reflect the sample numbers used for calculating the median values.

Figure 4. Temporal variations of $\delta^{13}C_{POM}$ (left) and $\delta^{15}N_{POM}$ (right) along the monitoring line (SI-line); (a) Monthly variation of $\delta^{13}C_{POM}$ in the surface layer, (b) monthly variation of $\delta^{15}N_{POM}$ in the surface layer, (c) monthly variation of $\delta^{13}C_{POM}$ in the subsurface layer, (d) monthly variation of $\delta^{15}N_{POM}$ in the subsurface layer, (e) yearly variation of $\delta^{13}C_{POM}$ in the surface during summer, and (f) yearly variation of $\delta^{15}N_{POM}$ in the surface during summer. Box plots show the mean (thick horizontal lines within boxes), standard deviation (boxes), maximum or minimum values (vertical bars), and outliers (closed circles). The lower-case italic characters near the boxes (x, y, and z) reflect the results of the pairwise test with Tukey–Kramer adjacent; the same character pairs showed an insignificant difference in the pair ($p > 0.05$). In the subsurface layer (c, d), the pairwise test with Tukey–Kramer adjacent was not significant among any pairs. The numbers just above the horizontal axis indicate the sample numbers.

Figure 5. (a) Diagram between $\delta^{15}N_{POM}$ and $\delta^{13}C_{POM}$. Stacked histograms of (b) $\delta^{13}C_{POM}$ and (c) $\delta^{15}N_{POM}$ for the two-dimensional Gaussian mixed model (GMM), with colors indicating the different classes.

Figure. 6. Differences in environmental parameters among the classes divided based on $\delta^{13}C_{POM}$ and $\delta^{15}N_{POM}$. Parameters include (a) temperature, (b) salinity, (c) nitrate concentration, (d) chlorophyll-*a* concentration, and (e) C:N ratio. Box plots show the mean (thick horizontal lines

within boxes), standard deviation (boxes), and maximum or minimum values (vertical bars). The small gray dots represent the raw values.

Figure. 7. (a) T–S (temperature–salinity) diagram overlayed with classification (I–IV) based on $\delta^{13}C_{POM}$ and $\delta^{15}N_{POM}$. In this diagram, salinity < 32 was not plotted. (b) An N-σ_t (nitrate-density) diagram. The nitrate concentration was transformed as a logarithm value.

Figure 8. The least-square mean (lsmean) based effects of the environmental parameters in the least AIC GLM for $\delta^{13}C_{POM}$. Effect of (a) classes, (b) sampling depth, (c) latitude, (d) temperature, (e) salinity, (f) log-transformed chlorophyll-*a* concentration, and (g) log-transformed nitrate concentration. Closed circles with bars or solid lines with shadows represent the lsmeans with 95 % confidence intervals. The small gray dots represent the observation data.

Figure 9. Least-square mean (lsmean) values based on the effects of the environmental parameters in the least-AIC GLM for $\delta^{15}N_{POM}$. Effect of (a) classes, (b) sampling seasons, (c) sampling depth, (d) latitude, (e) longitude, (f) temperature, and (g) salinity. Closed circles with bars or solid lines with shadows represent the lsmeans with 95 % confidence intervals. The small gray dots represent the observation data.

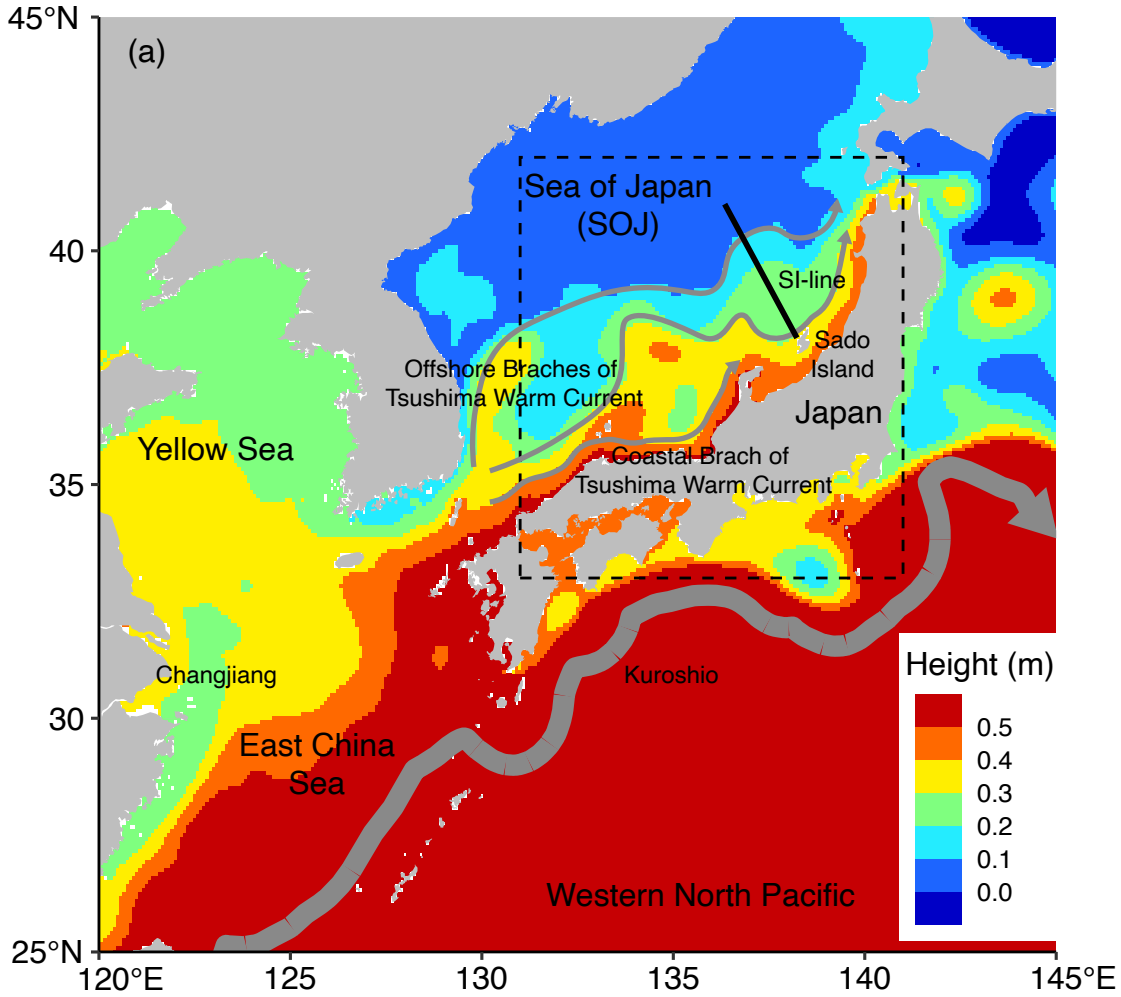
(a)
45°N
40
35
30
25°N
120°E
125
130
135
140
145°E
Sea of Japan
(SOJ)
SI-line
Sado
Island
Offshore Braches of
Tsushima Warm Current
Japan
Yellow Sea
Coastal Brach of
Tsushima Warm Current
Changjiang
Kuroshio
East China
Sea
Western North Pacific
Height (m)
0.5
0.4
0.3
0.2
0.1
0.0

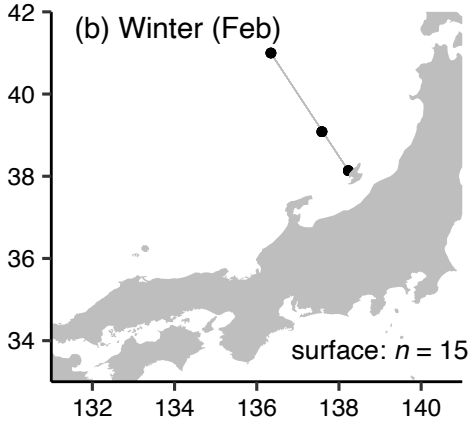
(b) Winter (Feb)
42
40
38
36
34
132
134
136
138
140
surface: n = 15

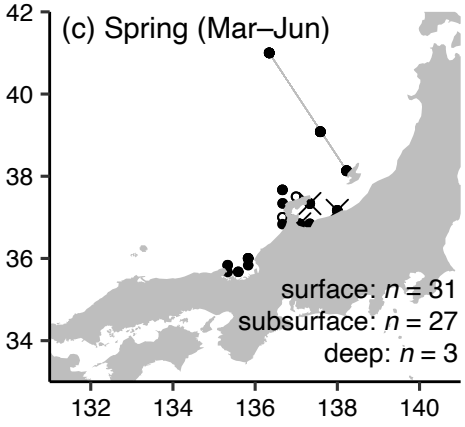
(c) Spring (Mar–Jun)
42
40
38
36
34
132
134
136
138
140
surface: n = 31
subsurface: n = 27
deep: n = 3

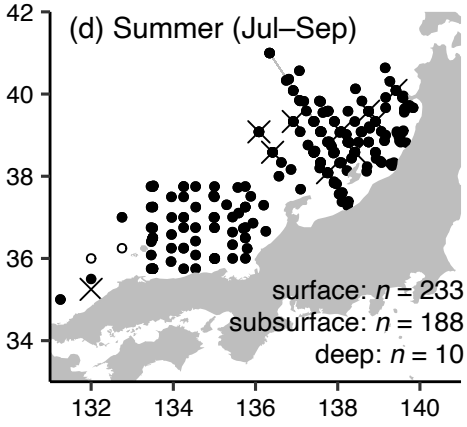
(d) Summer (Jul–Sep)
42
40
38
36
34
132
134
136
138
140
surface: n = 233
subsurface: n = 188
deep: n = 10

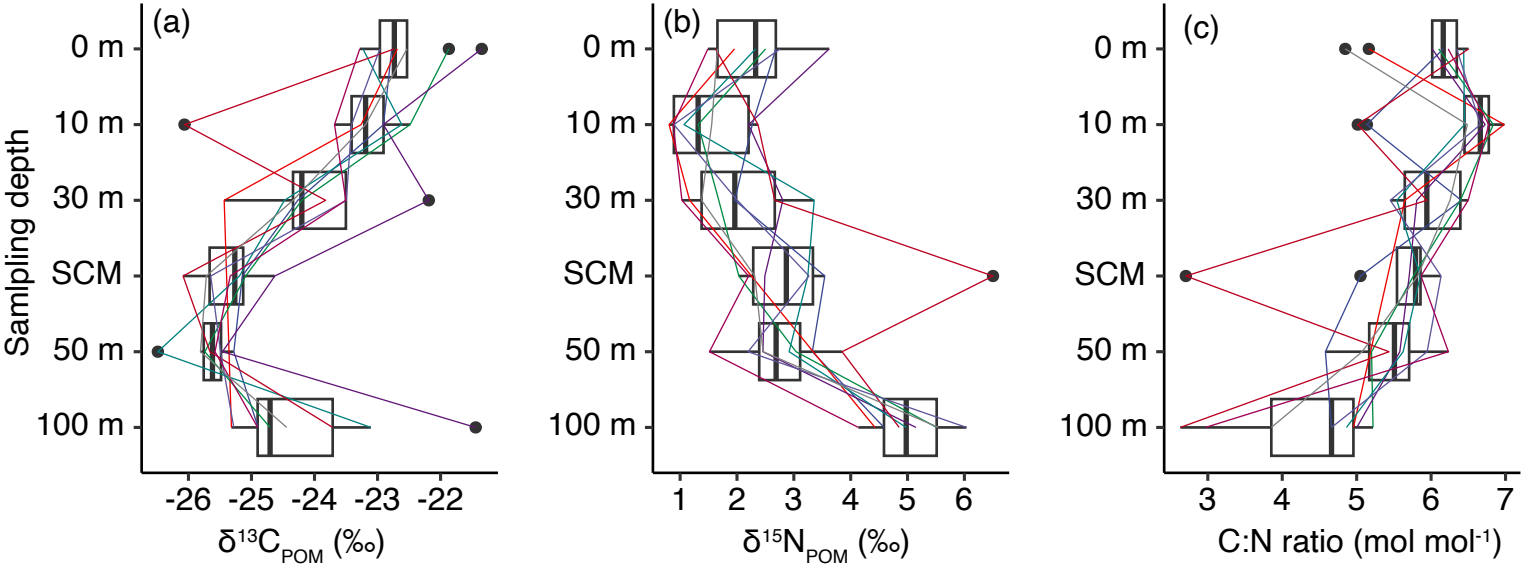
(a)
(b)
(c)
Samlpling depth
0 m
10 m
30 m
SCM
50 m
100 m
-26 -25 -24 -23 -22
1 2 3 4 5 6
3 4 5 6 7
δ13CPOM (‰)
δ15NPOM (‰)
C:N ratio (mol mol-1)

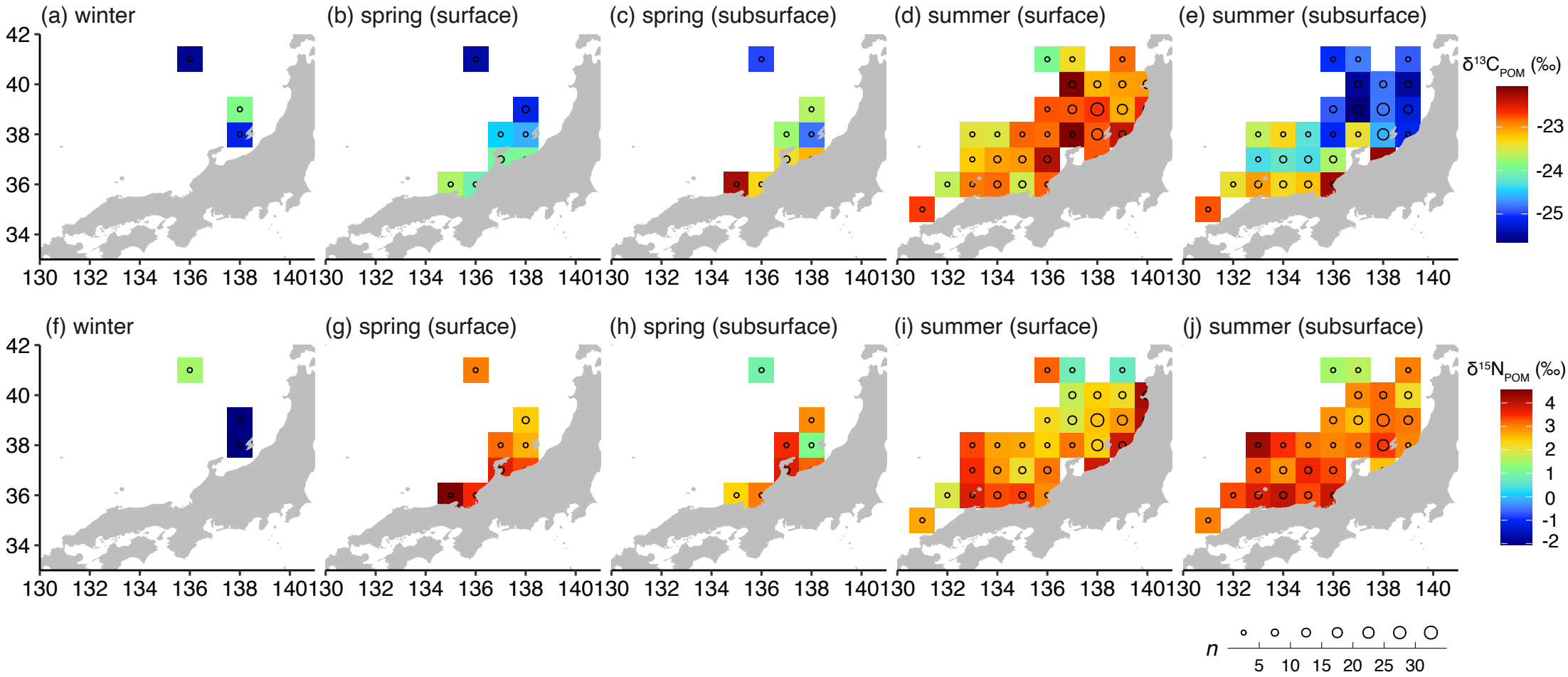
(a) winter
(b) spring (surface)
(c) spring (subsurface)
(d) summer (surface)
(e) summer (subsurface)
(f) winter
(g) spring (surface)
(h) spring (subsurface)
(i) summer (surface)
(j) summer (subsurface)
42
40
38
36
34
130 132 134 136 138 140
δ13CPOM (‰)
-23
-24
-25
δ15NPOM (‰)
4
3
2
1
0
-1
-2
n
5 10 15 20 25 30

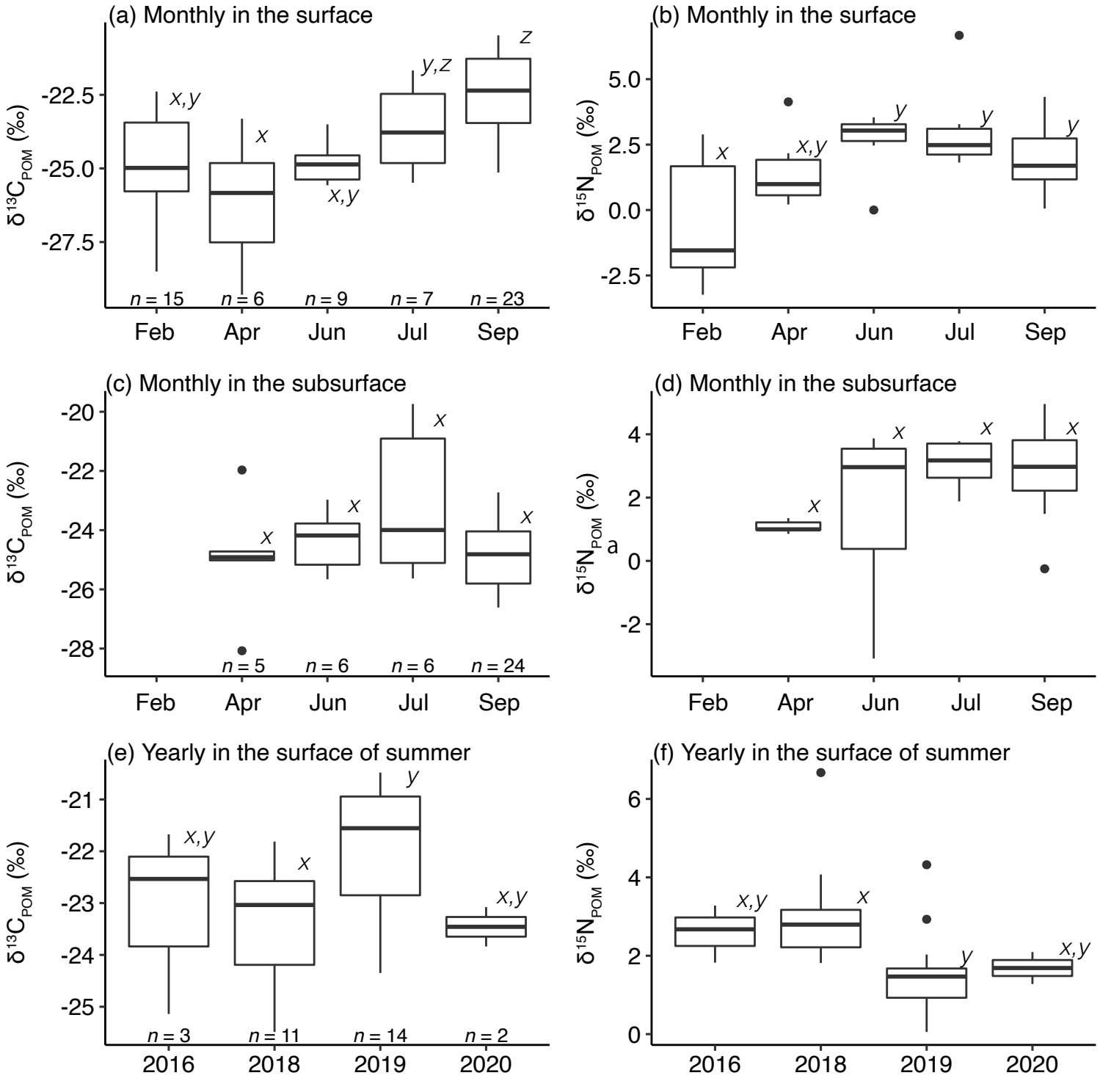
(a) Monthly in the surface
δ13CPOM (‰)
-22.5
-25.0
-27.5
x,y
x
x,y
y,z
z
n = 15
n = 6
n = 9
n = 7
n = 23
Feb
Apr
Jun
Jul
Sep
(b) Monthly in the surface
δ15NPOM (‰)
5.0
2.5
0.0
-2.5
x
x,y
y
y
y
Feb
Apr
Jun
Jul
Sep
(c) Monthly in the subsurface
δ13CPOM (‰)
-20
-22
-24
-26
-28
x
x
x
x
n = 5
n = 6
n = 6
n = 24
Feb
Apr
Jun
Jul
Sep
(d) Monthly in the subsurface
δ15NPOM (‰)
4
2
0
-2
x
x
x
x
Feb
Apr
Jun
Jul
Sep
(e) Yearly in the surface of summer
δ13CPOM (‰)
-21
-22
-23
-24
-25
x,y
x
y
x,y
n = 3
n = 11
n = 14
n = 2
2016
2018
2019
2020
(f) Yearly in the surface of summer
δ15NPOM (‰)
6
4
2
0
x,y
x
y
x,y
2016
2018
2019
2020

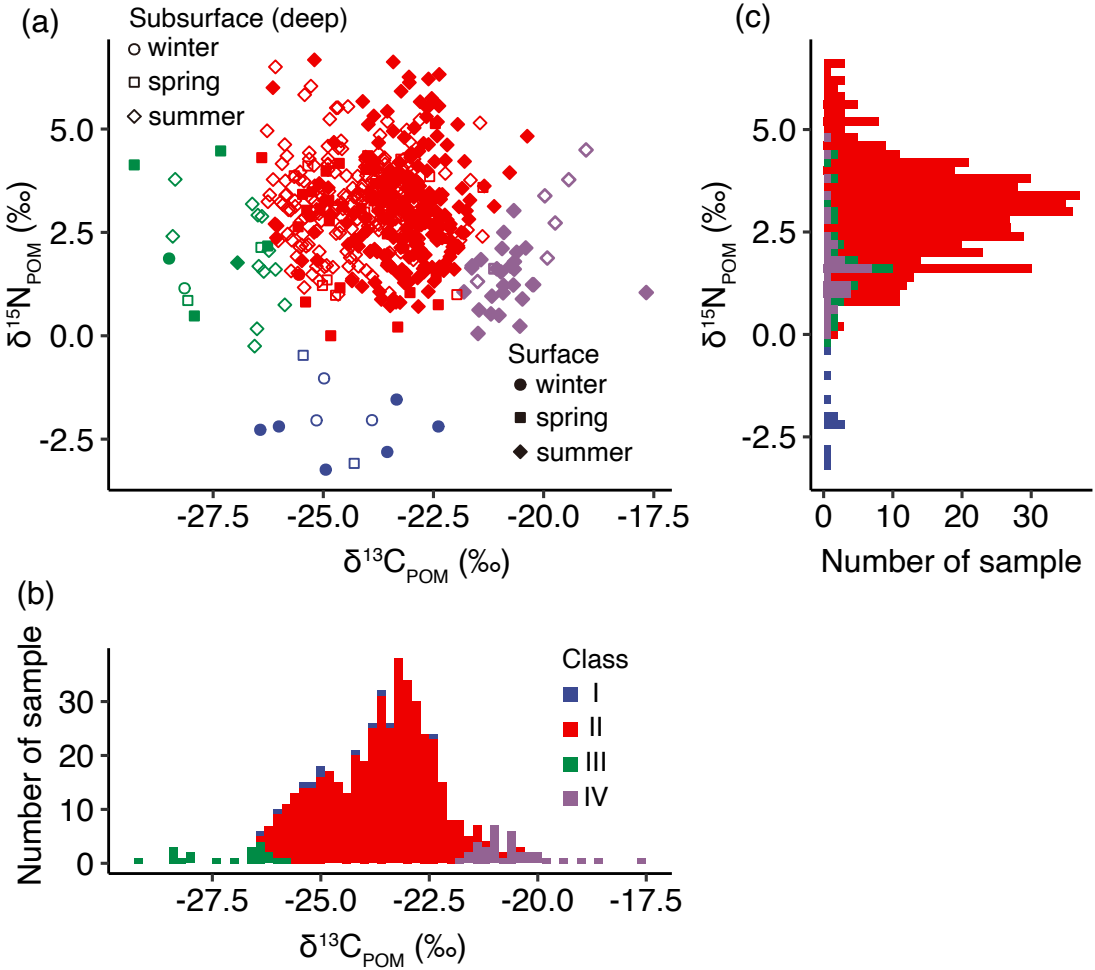
(a)
Subsurface (deep)
winter
spring
summer
Surface
winter
spring
summer
5.0
2.5
0.0
-2.5
δ15NPOM (‰)
-27.5
-25.0
-22.5
-20.0
-17.5
δ13CPOM (‰)
(c)
0
10
20
30
Number of sample
(b)
Number of sample
Class
I
II
III
IV

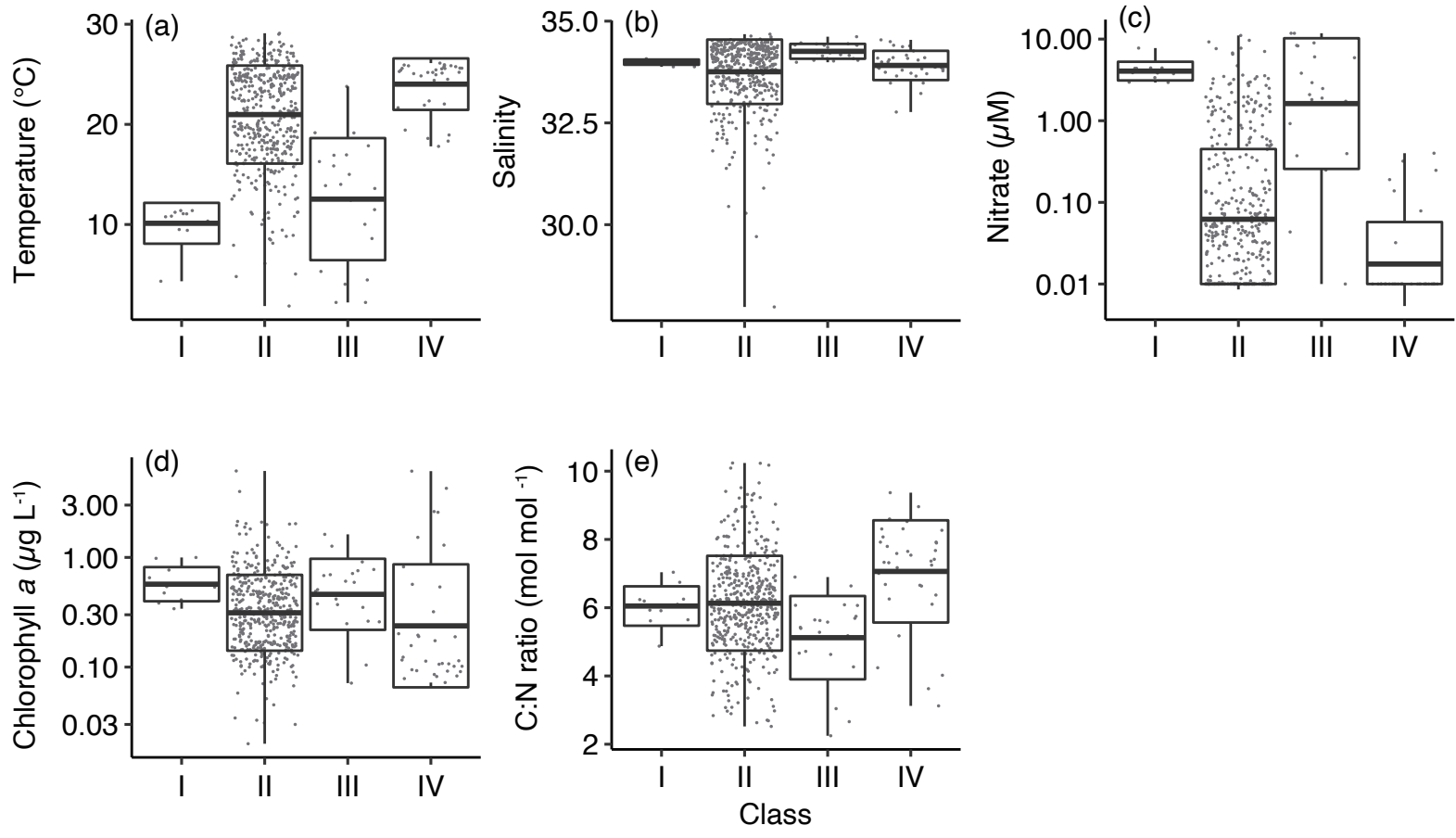
(a)
Temperature (°C)
30
20
10
I
II
III
IV
(b)
Salinity
35.0
32.5
30.0
(c)
Nitrate (μM)
10.00
1.00
0.10
0.01
(d)
Chlorophyll a (μg L-1)
3.00
1.00
0.30
0.10
0.03
(e)
C:N ratio (mol mol-1)
10
8
6
4
2
Class

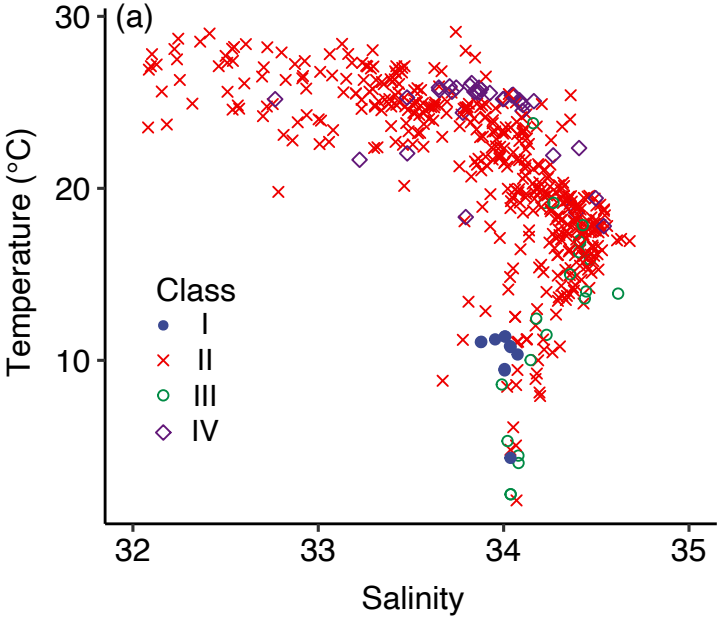
(a)
30
20
10
Temperature (°C)
Class
I
II
III
IV
32
33
34
35
Salinity

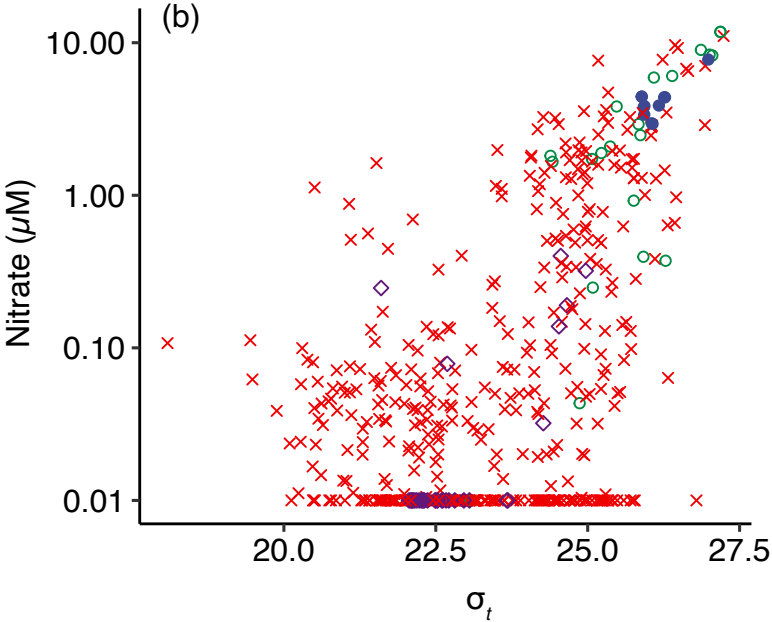
(b)
10.00
1.00
0.10
0.01
Nitrate (μM)
20.0
22.5
25.0
27.5
σt

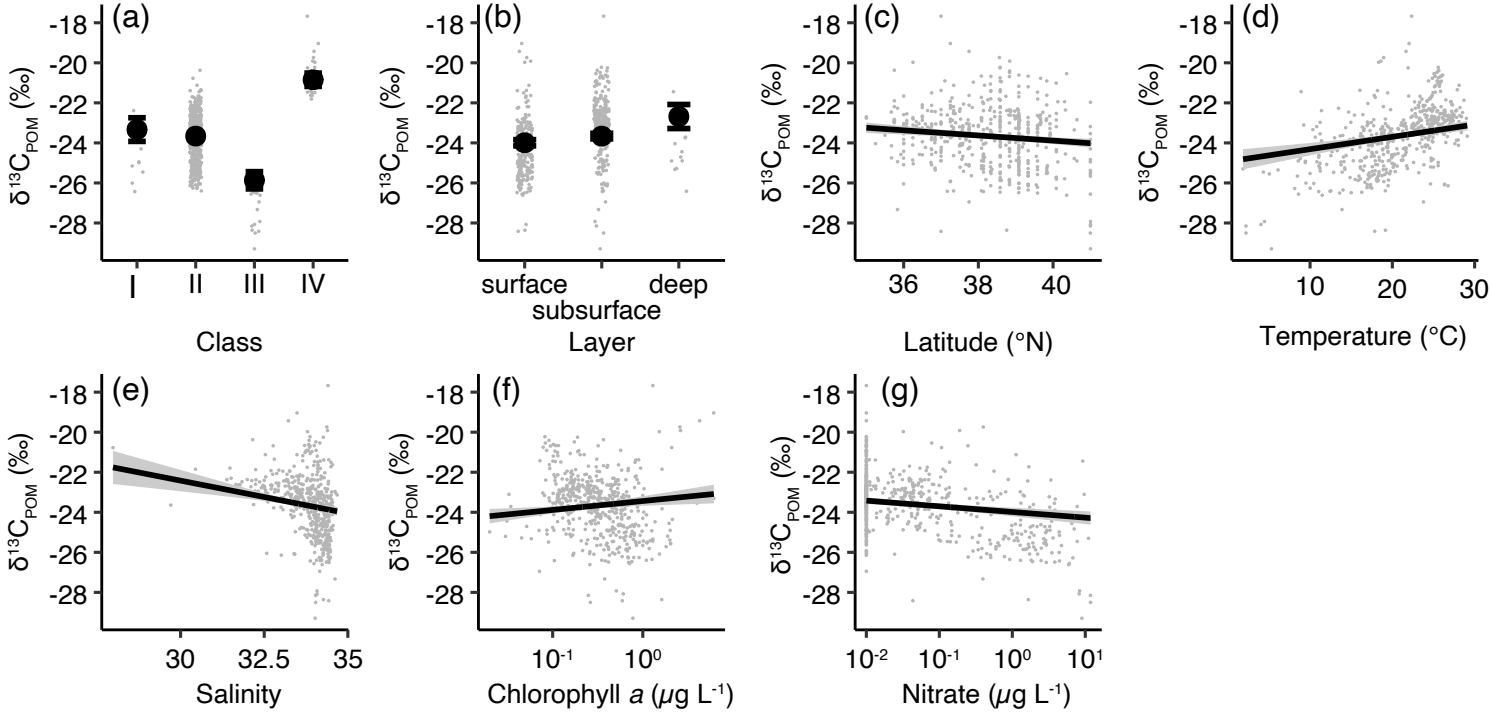
(a)
(b)
(c)
(d)
(e)
(f)
(g)
δ13CPOM (‰)
-18
-20
-22
-24
-26
-28
I
II
III
IV
Class
surface
subsurface
deep
Layer
36
38
40
Latitude (°N)
10
20
30
Temperature (°C)
30
32.5
35
Salinity
10-1
100
Chlorophyll a (μg L-1)
10-2
10-1
100
101
Nitrate (μg L-1)

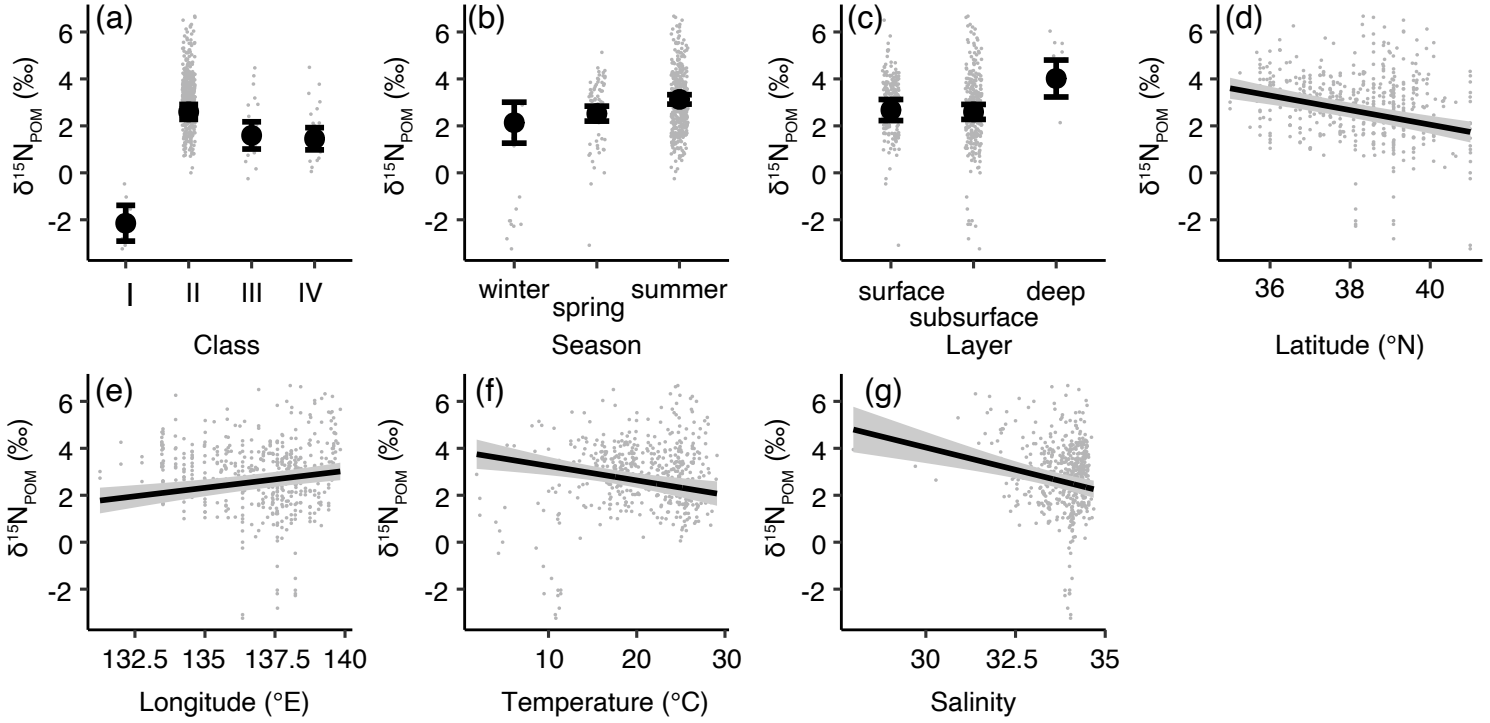
(a)
(b)
(c)
(d)
(e)
(f)
(g)
δ15NPOM (‰)
6
4
2
0
-2
I
II
III
IV
Class
winter
spring
summer
Season
surface
subsurface
deep
Layer
36
38
40
Latitude (°N)
132.5
135
137.5
140
Longitude (°E)
10
20
30
Temperature (°C)
30
32.5
35
Salinity